

# TABLE OF CONTENTS

<b>PREFACE</b> .....	<b>3</b>
<b>OBJECTIVES</b> .....	<b>5</b>
<b>1. INTRODUCTION</b> .....	<b>7</b>
1.1. SCATTEROMETER MISSIONS .....	7
1.2. NSCAT INSTRUMENT CHARACTERISTICS .....	7
1.3. THE RELATIONSHIP BETWEEN $\sigma^\circ$ AND WIND: THE GMF .....	9
1.4. THE $\sigma^\circ$ MEASUREMENT SPACE AND ITS PROPERTIES .....	10
<b>2. EVALUATION OF THE KU-BAND GMF AND THE NSCAT <math>\sigma^\circ</math> MEASUREMENTS BY USING THE MEASUREMENT SPACE</b> .....	<b>13</b>
<b>3. THE INVERSION PROBLEM AND THE NEED FOR A TRANSFORMED SPACE</b> .....	<b>19</b>
3.1. THE EXPERIENCE WITH ERS SCATTEROMETERS AND THE THEORETICAL APPROACH .....	19
3.2. PROPOSAL OF A NSCAT MEASUREMENT SPACE TRANSFORMATION .....	25
<b>4. NSCAT WINDS QUALITY CONTROL (QC)</b> .....	<b>29</b>
4.1. A QC BASED ON THE INVERSION: JUSTIFICATION OF THE APPROACH.....	29
4.2. THE INVERSION RESIDUAL AND ITS NORMALISATION: $R_N$ .....	29
4.3. CORRELATION BETWEEN THE NORMALISED RESIDUAL AND THE DEPARTURE FROM ECMWF WINDS .....	30
4.4. A CLOSER LOOK AT THE EFFECT OF RAIN.....	33
4.5. SEVERAL CASES TO ILLUSTRATE THE QC METHOD PERFORMANCE .....	34
4.6. THE WIND DIRECTION DEPENDENCY OF $R_N$ AND ECMWF-RMS.....	34
<b>5. SUMMARY AND CONCLUSIONS</b> .....	<b>39</b>
<b>6. ONGOING WORK AND PLANS FOR QUIKSCAT</b> .....	<b>41</b>
6.1. NSCAT WIND DIRECTION RETRIEVAL .....	41
6.2. IMPACT STUDY OF NSCAT WINDS IN WEATHER FORECAST .....	41
6.4. FOLLOW-ON ACTIVITIES AT KNMI .....	44
<b>REFERENCES</b> .....	<b>45</b>
<b>ACKNOWLEDGEMENTS</b> .....	<b>47</b>
<b>ACRONYMS</b> .....	<b>49</b>
<b>ANNEX 1: NSCAT MEASUREMENT SPACE TRANSFORMATION</b> .....	<b>51</b>
<b>ANNEX 2: NSCAT PROCESSING INFRASTRUCTURE DEVELOPED AT KNMI AND ECMWF</b> ...	<b>53</b>
<b>ANNEX 3: RELATED PRESENTATIONS AND PUBLICATIONS</b> .....	<b>55</b>
<b>ANNEX 4: CONTACTS AND COLLABORATIONS WITH OTHER RESEARCH GROUPS</b> .....	<b>57</b>



## Preface

The EUMETSAT NSCAT Fellowship has been carried out at the Royal Netherlands Meteorological Institute (KNMI) in De Bilt (The Netherlands), within the research group of the Satellite Data group of the Observations and Modelling department. The project started in February 1997 and had a duration of two years. The main goal during that time has been to get acquainted with Ku-band scatterometry and NSCAT in particular, using the experience gained in Europe through the ERS scatterometer missions.

The American scatterometer missions present a bridge to cover the gap between present and future European scatterometers. Therefore, EUMETSAT and KNMI invest through this and the QuikSCAT fellowship (starting February '99) in gaining knowledge on the use of Ku-band scatterometer data and the operational assimilation of scatterometer winds for weather forecasting. By doing so, the European involvement in spaceborne scatterometry and its application is ensured for the benefit of the European meteorological community.



# Objectives

The main goal of the NSCAT fellowship was to improve the understanding of NSCAT winds, in line with the experience gained in Europe on the ERS scatterometers. After the failure of ADEOS in June 1997, and the setup of the QuikSCAT mission, these objectives were extended to include Ku-band scatterometry in general, in order to prepare the grounds for an effective real-time assimilation of winds from a new concept scatterometer: SeaWinds on QuikSCAT.

The main areas investigated are the following:

- **Backscatter measurement ( $\sigma^0$ ) evaluation**
- **Geophysical Model Function (GMF) evaluation**
- **Inversion**
- **Wind Product Quality Control (QC)**

The measurement space, or ‘cone’ concept (chapter 1) is used to evaluate the consistency of  $\sigma^0$  measurements and their noise properties. It can also be used to evaluate the fit between the measurements and the **GMF** that relates the  $\sigma^0$  characteristics to the near surface wind vector (chapter 2).

The main assumptions made to define the **inversion** process are also evaluated. On one hand, the justification for an optimum inversion space is discussed and a measurement space transformation is suggested for NSCAT (chapter 3). On the other hand, the need for **wind QC** based on the inversion is justified and a method is proposed, which goes through an evaluation of the measurement noise characteristics. The effects of this QC are examined and compared with other wind quality information (chapter 4).

After the summary and conclusions (chapter 5), other ongoing work related to the subject is described (chapter 6), which focuses on open issues, the SeaWinds geometry and on scatterometer data assimilation in Numerical Weather Prediction (NWP) models.



# 1. Introduction

## 1.1. Scatterometer missions

After the successful flight of the Seasat scatterometer in 1978, both NASA and ESA have developed scatterometer missions. The NASA scatterometer NSCAT was launched on the Japanese satellite ADEOS-I in August 1996 and ceased to operate in June 1997, after a total power failure on the platform. The next NASA scatterometers will be SeaWinds on QuikSCAT, to be launched on May 16<sup>th</sup> 1999 and SeaWinds on ADEOS-II, after the summer of the year 2000. ESA launched its first scatterometer on the ERS-1 satellite in July 1991, which was switched into a stand-by mode in 1996, after five years of successful operation. A second and identical European scatterometer on ERS-2 was launched in April 1995 and operates fine up to this date. Programmed in the future of European scatterometry is ASCAT on board of the METOP-I, -II and -III platforms (2003).

NSCAT operates in the Ku frequency band, as do the rest of American scatterometers, whereas the European scatterometers work in C-band. NSCAT and the European scatterometers have been designed after the multiple fan beam illumination first tried with Seasat, while SeaWinds will operate with a scanning pencil beam illumination.

The most attractive feature of the NSCAT mission was its space/time coverage, which made the scatterometer mission potentially beneficial for operational use in weather forecasting [Stoffelen 1998]. Another interesting aspect of NSCAT is the possibility of having both horizontally- and vertically-polarised measurements, which opens up new possibilities in better solving the wind solution ambiguity problem. Both characteristics are also present in SeaWinds. This and the fact that the two instruments work in Ku-band, encourage a detailed study of the NSCAT GMF and inversion problem as a preparation for an early and effective use of good quality winds in meteorological analysis, from the future Seawinds on QuikSCAT. Moreover, the successful experience with the ERS scatterometers suggests a potential benefit from the further development of the ERS data processing methodology to improve the quality of NSCAT and SeaWinds retrieved winds.

## 1.2. NSCAT Instrument characteristics

A detailed description of the NSCAT measuring geometry is given in [Naderi, 1991]. Figure 1.1 shows the relative position of the six antenna illumination patterns on the ocean surface and the extensive coverage given by the two swaths swept on both sides of the track. The along-beam resolution is achieved by Doppler shift filtering and results in 25 km cells. The desired along-track resolution of 25 km size is achieved by measurement timing control. The combination of these two methods provides the geographical position of all the backscatter measurements from the different beams, which are binned into 50 km x50 km Wind Vector Cells (WVC). The WVC

distribution results in a succession of across-track rows, each one composed of 24 WVC, numbered from 1 to 24 from left to right. On each side of the swath, the fore, mid and aft antennas will be numbered as 1, 2 and 3 respectively. Each target on the surface is illuminated by the three antennae. All antennae take vertically polarised measurements (VV), and the mid antenna provides with an additional measurement with horizontal polarisation (HH). The different backscatter measurements will be denoted  $\sigma^{\circ}_1$ ,  $\sigma^{\circ}_{2V}$ ,  $\sigma^{\circ}_{2H}$  and  $\sigma^{\circ}_3$  for each WVC. When the  $\sigma^{\circ}$  WVC grouping algorithm has been applied, each WVC contains up to 6 different measurements from each beam, which results 24  $\sigma^{\circ}$  measurements in total. These measurements are generally not uniformly distributed with the WVC. For this study, the Level 1.7 NSCAT  $\sigma^{\circ}$  and the Level 2.0 NSCAT winds are used.

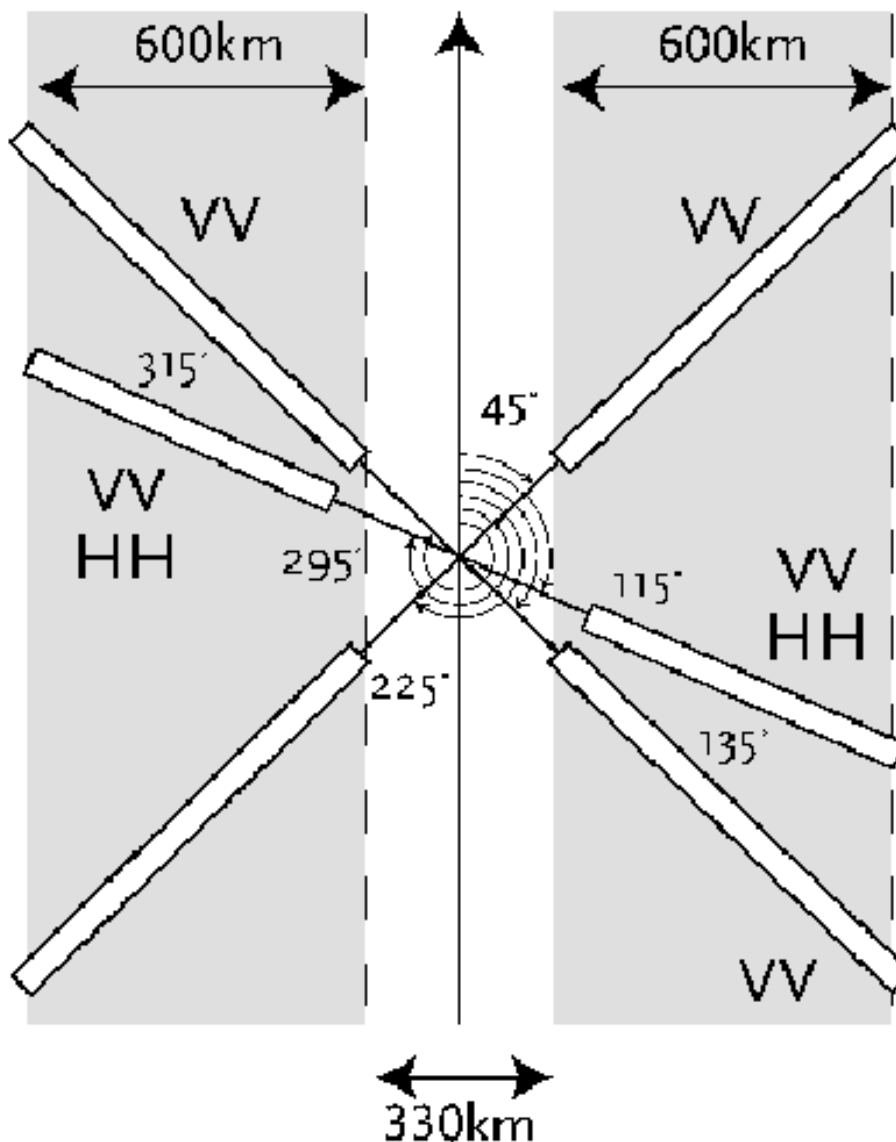


Figure 1.1: NSCAT antennae illumination pattern. The fore and aft antennae provide vertical polarisation measurements, while the mid antenna provides vertical and horizontal polarisation measurements, resulting in four different  $\sigma^{\circ}$  from each target over the ocean surface (From Stoffelen 1998)

### 1.3. The relationship between $\sigma^o$ and wind: the GMF

There is a physical relationship between the amount of backscattered microwave power and the wind near the ocean surface. Several attempts have been made to describe it theoretically, but the most common and successful approach so far is to derive it empirically. A general expression is

$$\begin{aligned}\sigma^o &= A_o + \sum_{i=1,5} A_i \cos(i\phi) \\ A_o &= a_o V^{\alpha_o} \\ A_i &= (a_i + \alpha_i \log V) A_o \\ a_o, a_i, \alpha_o, \alpha_i &= f(\theta, P)\end{aligned}\tag{Eq.1.1}$$

where V is the wind speed,  $\phi$  is the wind direction with respect to the antenna pattern over the surface,  $\theta$  is the incidence angle of the measurement and P is the antenna polarization. The measured backscatter therefore depends on two geophysical parameters (V,  $\phi$ ) and two parameters related to the geometry of the measurement system ( $\theta, P$ ). Dependencies on other geophysical parameters such as Sea Surface Temperature and Wave Age have proven to be small with respect to the wind dependency and no clear way of introducing them into the GMF has been found so far. For Ku-Band (14.6 GHz), the model coefficients are derived empirically for fair weather conditions, i.e., average sea state and in the absence of rain. Measurements taken in other more extreme conditions might therefore not represent the wind correctly through the GMF. In particular in the case of Ku-Band, it is known that rain affects the measured backscatter through a likely combination of two effects, namely the atmospheric attenuation of the microwave signal and the modification of the sea surface roughness by rain droplets. The wind retrieval in those special weather conditions has to be carefully considered when using the GMF as given above.

Several functions have been progressively tuned into the expression in [Eq:1.1] through the Seasat and NSCAT missions. The SASS-II GMF was derived using 3 months of Seasat measurements [Wentz *et al.*, 1984]]. Its derivation was based on the statistics of the SASS observations, and no *in situ* measurements were used, other than a mean global wind speed taken from climatology. After the first NSCAT calibration/validation meeting in January 1997, a new NSCAT-derived GMF called NSCAT-1 evolved from SASS-II. The modifications were based on collocation of numerical weather prediction near sea surface winds (10 m) and SSM/I wind speeds with NSCAT  $\sigma^o$  measurements [Wentz *et al.*, 1998]]. Both SASS-II and NSCAT-1 had only two harmonics. In 1998, a new tuning of the model using the whole mission of NSCAT data was done, resulting in NSCAT-2, which features five harmonics. The changes were motivated by improving the incidence angle dependency and adjusting the wind speed average to the one measured by buoys. NSCAT-2 is the GMF used for the last reprocessing of NSCAT data, and the best starting point for the retrieval of winds from SeaWinds on QuikSCAT.

## 1.4. The $\sigma^{\circ}$ measurement space and its properties

A method was developed for the ERS scatterometers to assess the quality of the backscatter measurements and the accuracy of the GMF [Stoffelen *et al.*, 1997, (1)]. When applied to backscatter measurements from the ocean surface, the analysis is based on the possibility of visualising triplets of  $\sigma^{\circ}$  measurements (corresponding to the fore, mid and aft beams) as a surface in a 3-D space. That surface is what we call the measurement space. The reason for that space being a surface is that the three  $\sigma^{\circ}$  measurements are related to two geophysical parameters: wind speed and wind direction. The mathematical expression of this surface is provided by the GMF.

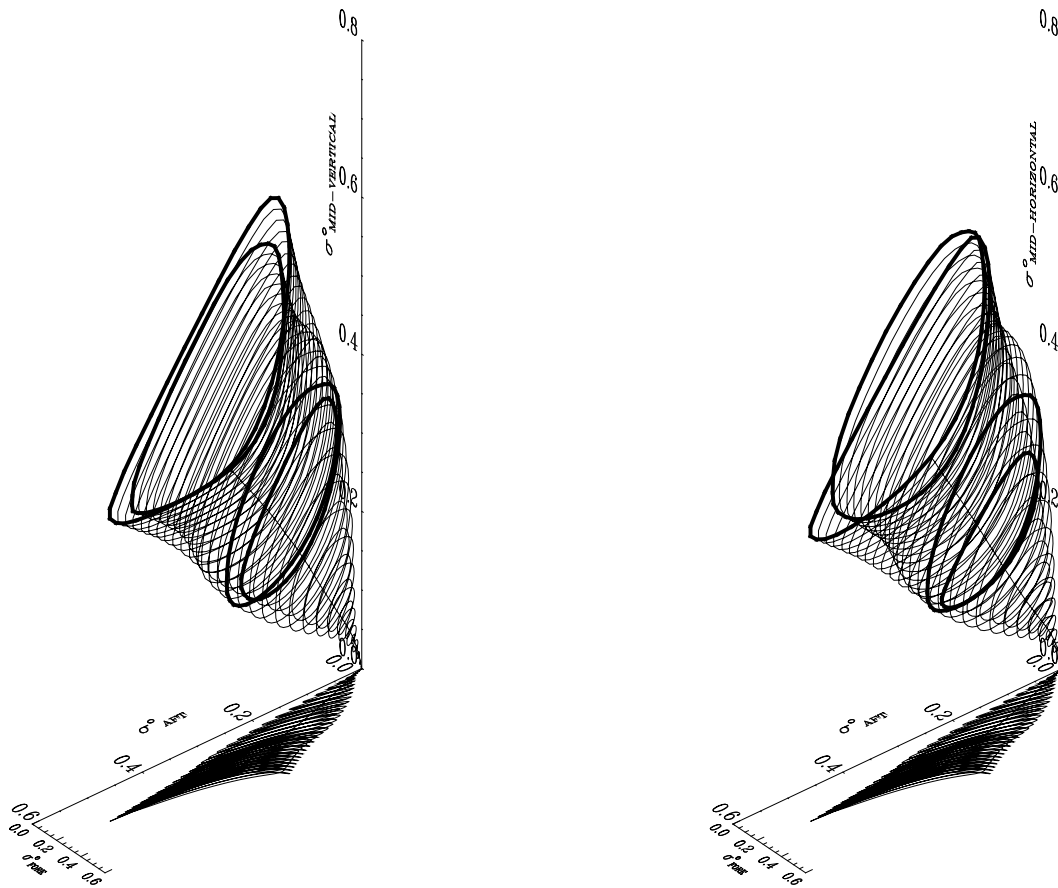


Figure 1.2: NSCAT-2 measurement space for node 9, represented in the 3-D subspaces  $(\sigma^{\circ}_1, \sigma^{\circ}_3, \sigma^{\circ}_{2V})$  and  $(\sigma^{\circ}_1, \sigma^{\circ}_3, \sigma^{\circ}_{2H})$  respectively. The location of measurements corresponding to wind speeds of 15 and 30 m/s has been highlighted. The incidence angle used is the average of the values found in all measurements within that node during one week of Level 1.7  $\sigma^{\circ}$ .

For every target over the ocean, NSCAT can take at least four backscatter measurements with different geometry, which correspond to the  $\sigma^0$  measurements from the four different combinations of antenna and polarisation. When plotted in a 4-D space they should also delineate a surface. It is very difficult to visualise a surface in a 4-D space, but it is possible to plot it in two meaningful subspaces  $[\sigma^0_1, \sigma^0_3, \sigma^0_{2V}]$  and  $[\sigma^0_1, \sigma^0_3, \sigma^0_{2H}]$  as in figure 1.2. For a given measurement geometry, this surface has roughly the shape of a two-sheath cone. The expression of the vector  $[\sigma^0_1, \sigma^0_{2V}, \sigma^0_{2H}, \sigma^0_3]$  is given by the GMF as

$$\begin{aligned}\sigma^o_1 &= A_o + \sum_{i=1,5} A_i \cos(i(\phi_2 + 70)) \\ \sigma^o_{2V} &= A_o ' + \sum_{i=1,5} A_i ' \cos(i\phi_2) \\ \sigma^o_{2H} &= A_o '' + \sum_{i=1,5} A_i '' \cos(i\phi_2) \\ \sigma^o_3 &= A_o + \sum_{i=1,5} A_i \cos(i(\phi_2 - 20))\end{aligned}\tag{Eq.1.2}$$

where  $\phi_2$  is the wind direction angle with respect to the mid beam and the coefficients are calculated for the corresponding incidence angle and polarisation of each beam. Two different contributions can be distinguished to the vector  $[\sigma^o_1, \sigma^o_{2V}, \sigma^o_{2H}, \sigma^o_3]$ . The  $A_o$  term is mainly contributing to the length of the total vector and carries most of the wind speed dependency. That term is approximately defining the distance along the axis of the cone. The harmonic terms provide the modulation across the axis of the cone and builds up the two sheaths of the cone around that axis. Each sheath corresponds to a  $\phi_2$  interval of  $[-90,90]$  and  $[90,270]$  degrees respectively. For each node, the cone and its properties are examined in an effective way by slicing it in two types of cross-sections. One of them would contain the cone axis and would give information about the wind speed-dependent properties, and the other one would be normal to the axis and give the wind direction-dependent properties [Stoffelen *et al.*, 1997, (1)].

The experience with the ERS and Seasat scatterometers has shown that the main concern about the accuracy of the wind retrieval is related to wind direction, which does not only depend on the accuracy of the GMF, but also on the formulation of the wind retrieval problem itself (Stoffelen *et al.*, 1997 (2)) . For that reason, in the case of NSCAT we have focused on studying the cross sections normal to the cone.



## 2. Evaluation of the Ku-band GMF and the NSCAT $\sigma^\circ$ measurements by using the measurement space

In order to simplify the visualisation of the measurement space, let us consider the cone in 3-D space represented by the  $[\sigma_1^\circ, \sigma_3^\circ, \sigma_{2V}^\circ]$  triplets (fig 1.2). Vertical cross-sections (approximately normal to the cone axis) are defined by their distance to the centre of co-ordinates D, measured in the plane  $[\sigma_1^\circ, \sigma_3^\circ]$ . Using [Eq:1.2] we can derive an expression for D, which appears to be mainly related to wind speed:

$$D = \frac{(\sigma_1^\circ + \sigma_3^\circ)}{\sqrt{2}}$$

$$D \approx A_o \sqrt{2}$$

[Eq:2.1]

In order to make this approximation, it is necessary to assume that the  $A_1$  term can be neglected with respect to the term  $A_o$ . This was shown to be the case for ERS in Stoffelen *et al.*, 1997 (2). In the case of NSCAT, Wentz *et al.*, 1998 shows that for horizontal polarisation  $A_1$  is slightly higher. Within those sections, triplets can be visualised in the following axis system, contained in the cross-section:

$$x = \frac{(\sigma_3^\circ - \sigma_1^\circ)}{\sqrt{2}}$$

$$y = \sigma_{2V}^\circ - E[\sigma_{2V}^\circ]$$

[Eq:2.2]

where  $E[\sigma_{2V}^\circ]$  is the expected mean value of  $\sigma_{2V}^\circ$ . Similar cross-sections can be drawn using  $\sigma_{2H}^\circ$  instead of  $\sigma_{2V}^\circ$ . In the vertical axis we find information corresponding to the mid beam, while in the horizontal axis we have information about the difference in measurement between the fore and aft beams. Some of these sections are found in figure 2.1.

Sections built up by using  $\sigma_{2V}^\circ$  or  $\sigma_{2H}^\circ$  are very similar for low incidence angles and high wind speeds, i.e., high D (fig 2.1(top)). They differ a lot at high incidence angles and mid to low wind speeds, where the vertical component in the  $\sigma_{2V}^\circ$  plot tends to be flatter, since the horizontally polarised backscatter is weaker than the vertically polarised (fig 2.1(mid)). For mid to low wind speeds, the upwind and downwind cross-section loops when using  $\sigma_{2H}^\circ$ , are clearly separated (fig 2.1(bottom)). In the case of the sections using  $\sigma_{2V}^\circ$ , this is not the case in general, but only happens for some combinations of wind speed and node. The situations where the upwind and downwind cone sheaths can be clearly distinguished have potentially an effective ambiguity removal implicit in the inversion scheme.

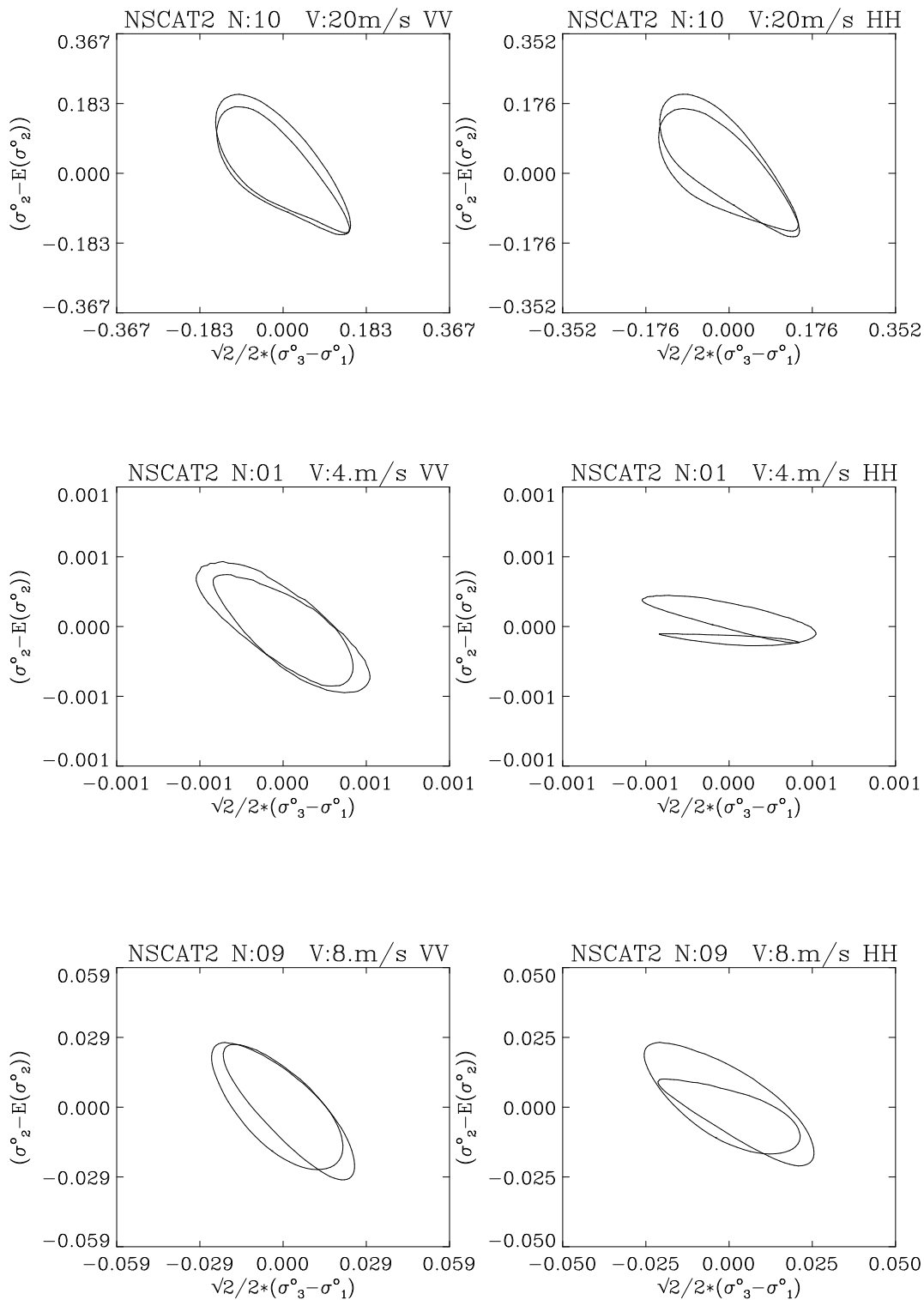


Figure 2.1: Three vertical cross-sections of the measurement spaces from figure 1.2. They correspond, from top to bottom, to nodes 10, 1 and 9 and to approximated wind speeds of 20, 4 and 8 m/s respectively. We have used either the vertical (VV) or the horizontal (HH) polarisation measurements from the mid beam, in left and right plots respectively.

Figure 2.2 shows  $\sigma^o$  triplets from batch S28 of the Level 1.7 data product, plotted ver NSCAT-2 GMF cross-sections similar to those in figure 2.1. The triplets are selected in a certain section of the model when they lie within a slice of  $0.006D$  thick around the section, which is within the expected measurement noise.

The fit of the data to the model cross-sections can be examined through two aspects. First, systematic misfits indicate errors in the modelling of the wind vector to radar backscatter relationship. These indicate to what extent NSCAT-2 may be improved in order to better model the measurements. We found that this is a typical case at the inner nodes, where a clear coherence in the position of the data is present, but which the GMF fails to fit (fig 2.2(top)). For mid to high wind speeds, we find in the other nodes a good fit between the model and the data (fig 2.2(mid)). For low wind speeds, the scatter is so big that it is very difficult to see where the GMF cone really lies, although considering the noise, a reasonable fit exists.

It is necessary at this point to clarify an aspect of the cross-sections that might lead to confusion when interpreting the scatter of the measurements in the plots. We build up the GMF cross-section using an average incidence angle per beam for that node. Without any correction, triplets with incidence angles slightly different from the expected mean defining the cross-section would generally not fit the GMF cone, since, according to their incidence angle, they belong in fact to a different cone. This misplacement is seen on the cross-section as a misfit and interpreted as measurement noise. Therefore, an incidence angle correction is performed, by simply normalising the  $\sigma^o$  by the  $A_o$  corresponding to that same wind speed, measured under the mean incidence angle of the section  $\theta_m$ .

$$\sigma_N^o(V, \phi, \theta) = \frac{A_o(V, \theta_m)}{A_o(V, \theta)} \sigma^o(V, \phi, \theta)$$

[Eq:2.3]

This correction makes triplets more representative for the cone to which they correspond according to their node number. As a test of the correction, figure 2.3 shows how the correction is applied to a set of  $\sigma^o$  triplets. The triplets have been simulated from a random field of wind vectors using NSCAT-2, by assuming that the incidence angle has a normal distribution with mean and standard deviation estimated for each node from a month of NSCAT data. Figure 2.3 shows how the incidence angle correction improves the fit of the GMF. It also shows that the magnitude of the correction is comparable to the measurement noise, thus it is important to apply it before assessing the measurement noise from the cross-sections.

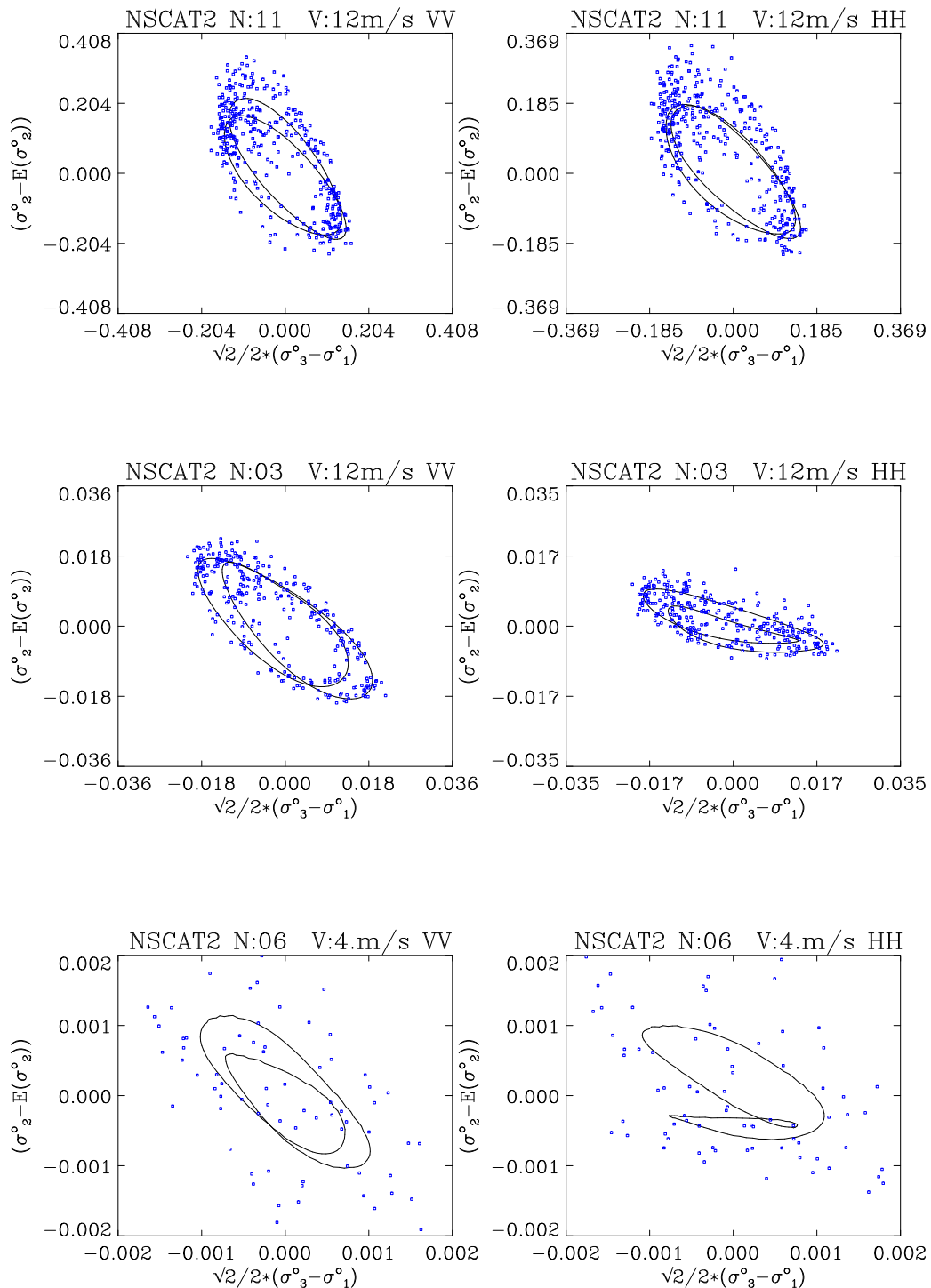


Figure 2.2: As figure 2.1, except including NSCAT  $\sigma^o$  measurements from Level 1.7 product, averaged over a WVC. The measurements correspond to three days at the beginning of March 1997, and they include an incidence angle correction with respect to the average value for that node.

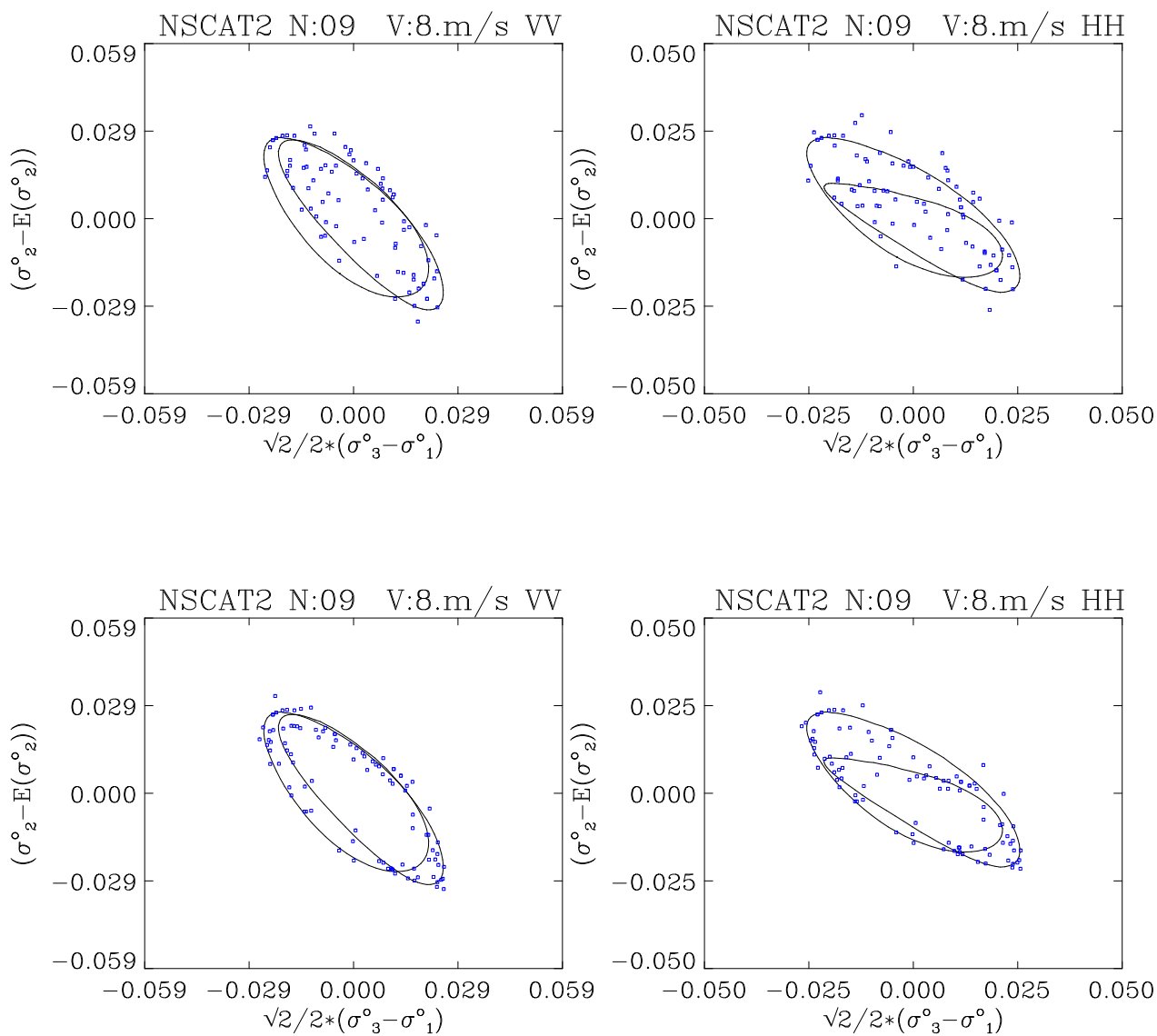


Figure 2.3: As in figure 2.2 for node 9 and wind speed of approximately 8 m/s (top) without incidence angle correction and (bottom) with incidence angle correction.



### 3. The inversion problem and the need for a transformed space

#### 3.1. The experience with ERS scatterometers and the theoretical approach

The wind retrieval is an inversion problem at each WVC that, given a set of measurements  $\sigma_{oi}^o$ , finds there wind vector  $(V, \phi)$  that, according to the GMF [Eq:1.1], has the highest probability of representing the true wind. Any inversion problem presented in these probabilistic terms can be formulated as the minimisation of a cost function  $J$  (also called MLE), which in case of the NSCAT wind retrieval has the following expression:

$$J(V, \phi) = \sum_{i=1}^N \left[ \frac{\sigma_{oi}^o - \sigma_{si}^o(V, \phi)}{SD(\sigma_{si}^o(V, \phi))} \right]^2$$

$$\sigma_{si}^o = GMF(V, \phi)$$

[Eq:3.1]

where  $\sigma_{si}^o$  is the backscatter simulated through the GMF for different trial values of  $(V, \phi)$ ,  $SD(\sigma_{si}^o)$  is the corresponding expected standard deviation and  $N$  is the number of measurements within the WVC.

$J$  is thus a distance to the GMF cone in a normalised  $N$ -dimensional space. This normalisation can be considered as similar to a scaling of the axes in the 4-D  $\sigma^o$  measurement space [Stoffelen *et al.*, 1997 (1)]. Thus it represents the way the distances in the measurement space are penalised in the inversion. If we scale the measurement space according to  $J$ , then we should have a space where the most probable solution for a given scaled triplet is the geometrically closest distance to the scaled cone surface.

This aspect has been studied by Stoffelen *et al.*, 1997 (1) for ERS-1 and it is illustrated in figure 3.1. Figure 3.1(a) would represent the measurement space, while figure 3.1(b) shows the triplets scaled by the expected noise, as provided by  $J$ . The latter would therefore represent the space used to compute the distances, proposed by [Eq:3.1]. Considering how the position of the triplets in this cross-section is modelled in [Eq:1.2], one can easily observe that for the retrieval of a realistic wind direction probability density function after the inversion, it is necessary that equal portions of the triplets are thrown onto equal wind direction intervals ( $\alpha$  in figure 3.1). This is achieved for a cone geometry with a rather constant curvature, i.e., circular. Having this in mind, normalisation by the measurement does not look favourable from the inversion point of view.

We are now going to explain the problem using probability theory, as it is approached in [Stoffelen *et al.*, 1997(1), appendix C]. What we want to evaluate is the probability of a true  $\sigma^o$  vector that we know should lie on the cone surface ( $\sigma_s^o$ ) given a measured  $\sigma^o$  vector ( $\sigma_o^o$ ). According to Bayes probability theorem, this can be written as:

$$p(\sigma_s^o | \sigma_o^o) = p(\sigma_o^o | \sigma_s^o) \frac{p(\sigma_s^o)}{p(\sigma_o^o)}$$

[Eq:3.2]

where  $p(\sigma_s^o | \sigma_o^o)$  is the conditional probability density of  $\sigma_s^o$  given a fixed  $\sigma_o^o$ ,  $p(\sigma_s^o)$  is the probability density of the true  $\sigma_o^o$  vector and  $p(\sigma_o^o)$  is the probability density of the measured  $\sigma^o$  vector, which in this process is a constant, since  $\sigma^o$  is given. In [Eq:3.2],  $p(\sigma_s^o)$  contains the *a priori* information about the probability of finding a triplet somewhere in the 4-D space.

Solving the inversion problem means finding the  $\sigma_s^o$  for which such  $p(\sigma_s^o | \sigma_o^o)$  is maximum. By maximising [Eq:3.2], an expression of  $J$  to be used in the inversion is obtained. In that process, two assumptions about the terms included in [Eq:3.2] can be made. First, there is no *a priori* information about the probability density of a given true triplet in the 4-D measurement space, and  $p(\sigma_s^o)$  is taken constant. Therefore, the problem comes down to maximising  $p(\sigma_o^o | \sigma_s^o)$ . [Eq:3.2] is then expressed as

$$p(\sigma_o^o | \sigma_s^o) = \frac{\text{EXP} \left\{ - \frac{(\sigma_o^o - \sigma_s^o)^2}{2(\text{SD}(\sigma_s^o))^2} \right\}}{\sqrt{(2\pi)} (\text{SD}(\sigma_s^o))^2}$$

[Eq:3.3]

and by maximising the logarithm of that expression, [Eq:3.1] is derived. When assuming proportional errors, an additional term  $\Sigma \{ \ln[\text{SD}(\sigma_{si}^o)]^2 \}$  is in fact added to the expression of  $J$  given in [Eq:3.1]. However, it has been verified that its contribution is mostly constant and does not affect the wind retrieval significantly. Therefore, it is not anymore considered for NSCAT wind retrieval by JPL.

Let us examine the first of the two assumptions with the help of figure 3.1. The probability density of a true triplet in the cross-section of figure 3.1(b),  $p(\sigma_s^o)$ , will be 0 for points out of the GMF cross-section. For points belonging to the GMF cone, the probability density of a true triplet should be constant for very  $\alpha$ , since we know that some wind directions do not prevail with respect to others. But looking at figure 3.1(b), this is clearly not the case. The cause is that the error distributions are mapped through a curved cone surface in the inversion, where the curvature varies with wind direction.

Stoffelen *et al.*, 1997 (1) conclude that  $J$  in [Eq:3.1] is not optimum for the inversion of the ERS-1 measurement space. The consequence for the inversion in the case of ERS-1 is shown in figure 3.2(a), where a wind direction distribution calculated from winds retrieved in the space shown in figure 3.1(b) is plotted. A transformation of the measurement space was proposed to solve this problem ( $Z = (\sigma^o)^{0.625}$ ), and it is shown in figure 3.1(c). The improvement in the wind direction distribution of the retrieved winds can be appreciated in figure 3.2.(b).

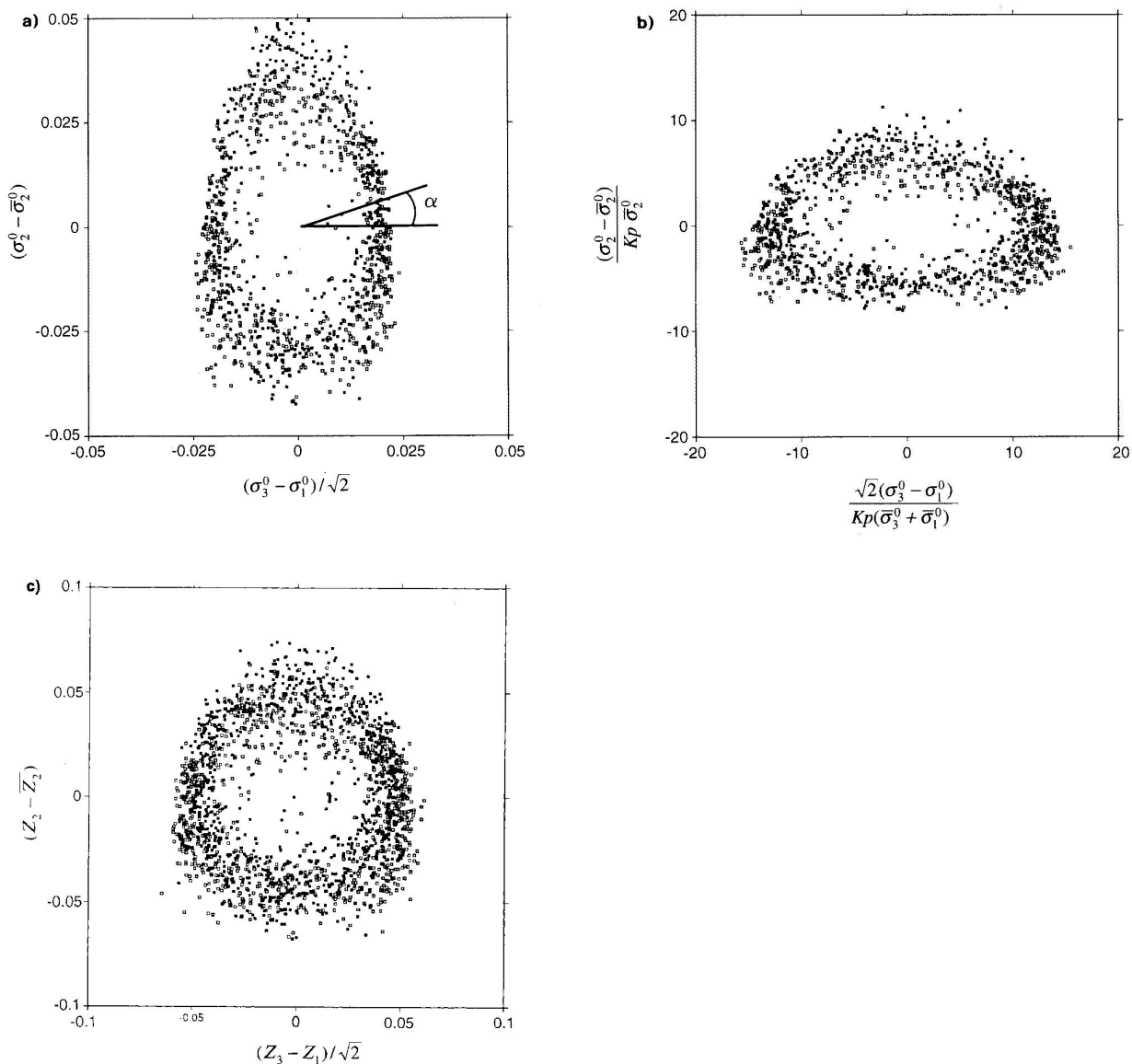


Figure 3.1: (taken from Stoffelen *et al.*, 1997 (1)). Cross section through 3D measurement space for  $(\sigma^o + \bar{\sigma}^o) = D\sqrt{2} = \text{constant}$ , with a thickness of  $0.005D$  for node 7. In (a) no scaling is used, in (b)  $\sigma_1^o$ ,  $\sigma_2^o$  and  $\sigma_3^o$  values are scaled by the measurement noise, and in (c) the cut is made in a transformed space where the axes are  $z_i = (\sigma^o)^{0.625}$ . Data from September 1993. It can be seen that the section (c) has the most symmetric properties.

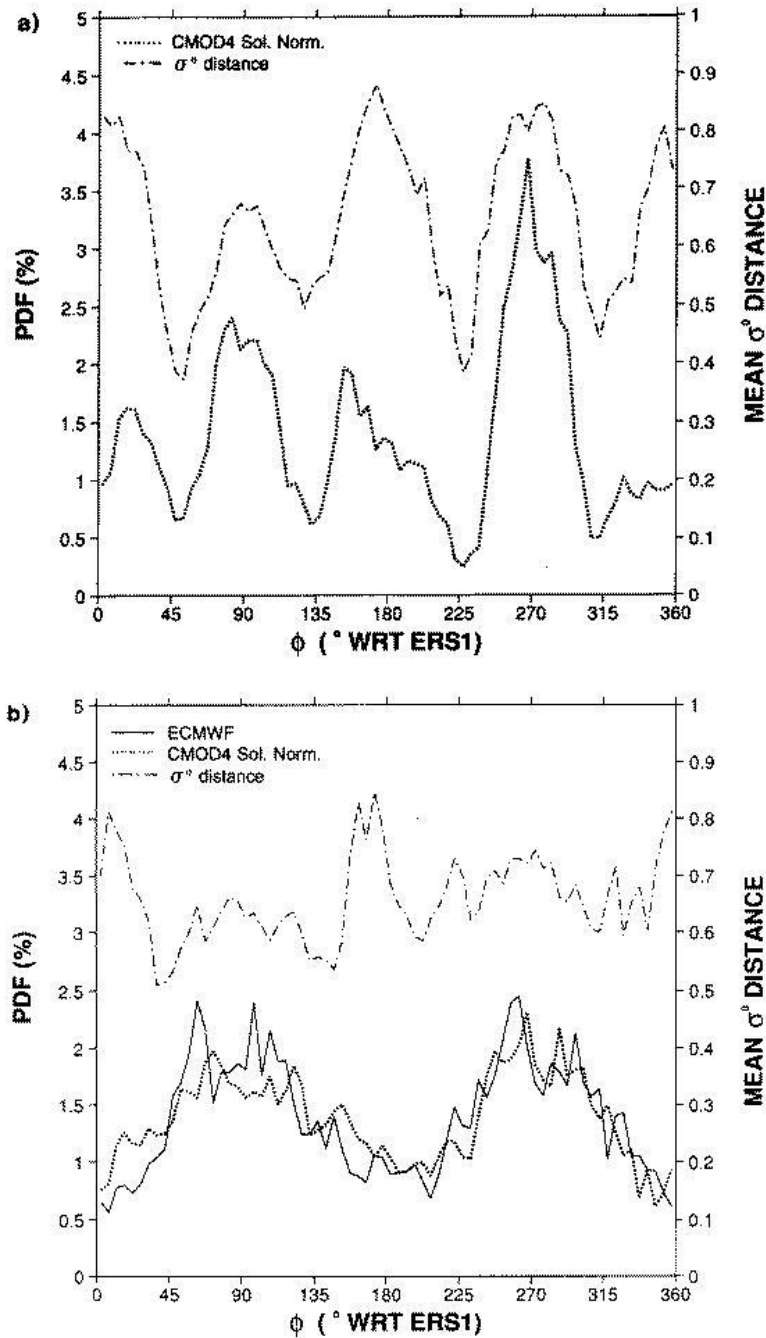


Figure 3.2: (taken from Stoffelen et al., 1997 (1)). Comparison of scatterometer direction distribution (a) when using inversion with normalisation by the measurement noise and (b) when using inversion in the transformed space. Wind direction is with respect to the satellite track. The solid line in (b) represents the ECMWF direction distribution and the dotted line the scatterometer distribution. The dash-dotted curve describes the mean distance to the cone in arbitrary unites (square root of the MLE). Data for node 3 for average wind speeds above 4 m/s and from 13 February 1994 2100 UTC to 16 February 1994 0900 UTC. In (a) the scatterometer wind direction distribution shows marked peaks and troughs approximately  $90^\circ$  apart, as so does the mean distance to the cone. In (b) in contrast, the scatterometer wind distribution is more realistic and indeed resembles the ECMWF angular distribution rather well, while the mean distance to the cone is much more uniform.

Inverted (NSCAT-2) (solid) vs Level20 (NSCAT-2) wind direction

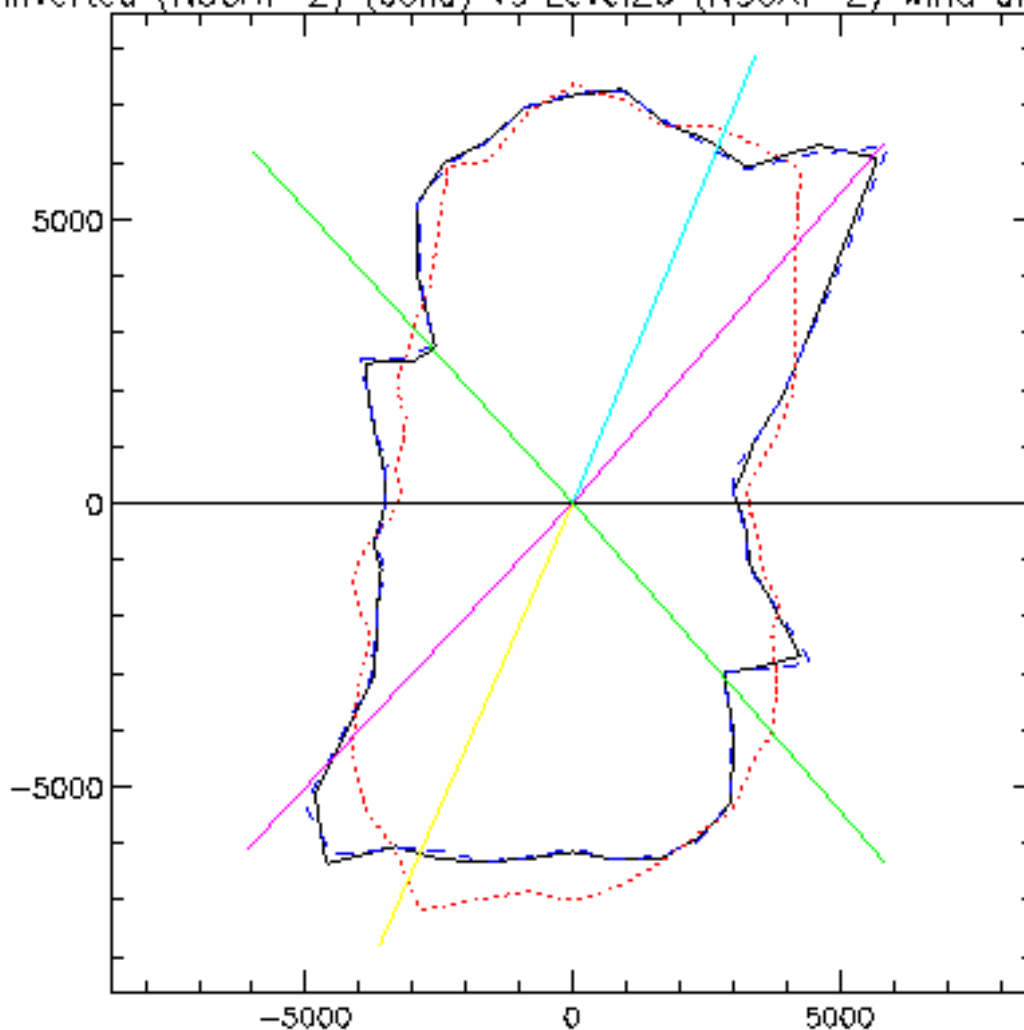


Figure 3.3: Polar histogram of the wind direction with respect to the satellite track. The black solid straight line represents the satellite track, and the coloured straight lines are the antennae patterns. The distance between the centre of co-ordinates and the curves represents the number of solution for each relative wind direction. For a week of data, the black curve corresponds to the winds retrieved by our inversion software, which is virtually identical to the winds contained in the JPL Level 2.0 product (in blue). The red dotted curve corresponds to collocated ECMWF winds.

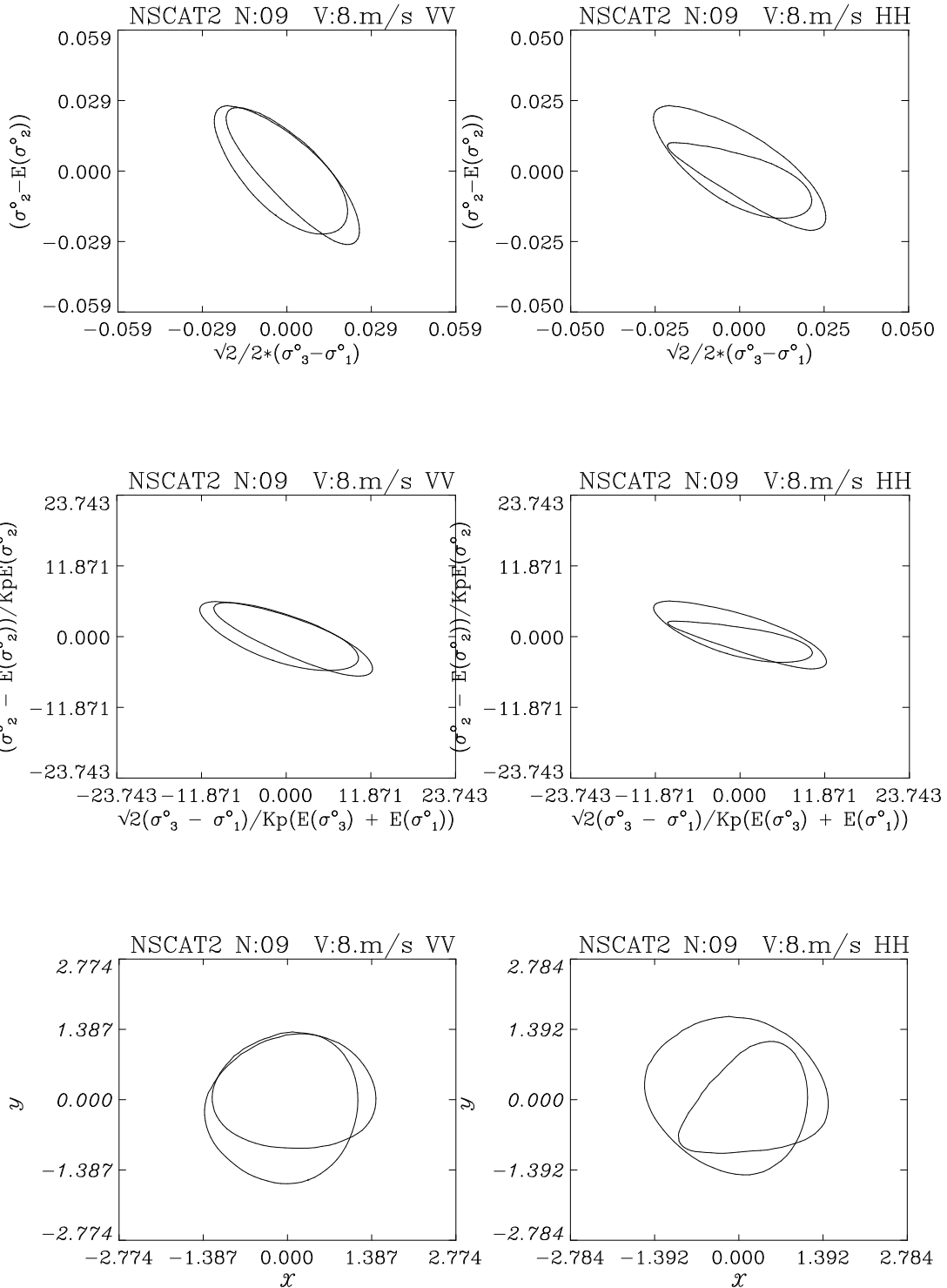


Figure 3.4: (Top) Vertical cross-section of the NSCAT-2 measurement spaces from figure 2.1., corresponding to node 6 and approximate wind speed of 8 m/s. (Mid). Vertical cross-sections of the NSCAT-2 measurement spaces normalised by the measurement noise estimation (the space used in the inversion (Eq.3.1)). (Bottom) Vertical cross-section of the NSCAT-2 transformed space proposed.

### 3.2. Proposal of a NSCAT measurement space transformation

In the case of NSCAT, the distribution of wind direction after the inversion (figure 3.3) indicates that there is still room for improvement in the wind retrieval accuracy, since this distribution is aligned with the antennae pattern. Figure 3.4(mid) shows how the NSCAT  $\sigma^o$  space looks after normalisation by  $SD(\sigma_{si}^o)$ , as proposed in the inversion formula. The cone is skewed and not symmetric. It is therefore necessary to perform a transformation of the measurement space to achieve a more circular distribution of the triplets over the cross-sections. The result of a transformation that we propose can be seen in figure 3.4(bottom) for a particular WVC and D.

The suggested transformation is based on decoupling the  $V, \phi$  dependency of  $\sigma^o$ , and then transforming the measurement space in order to achieve a constant probability density of the triplets with respect to the wind direction, much like as was done for ERS.

The first step implies subtracting the  $A_o$  term, and normalising by the  $A_2$  coefficient.

$$\begin{aligned} x &= \frac{\sigma_1^o - A_o}{A_2} \approx -\text{COS}(2\phi_2 - 40) \\ y &= \frac{\sigma_{2V}^o - A_o}{A_2} \approx \text{COS}(2\phi_2) \\ z &= \frac{\sigma_{2H}^o - A_o}{A_2} \approx \text{COS}(2\phi_2) \\ t &= \frac{\sigma_3^o - A_o}{A_2} \approx \text{COS}(2\phi_2 - 40) \end{aligned}$$

[Eq:3.4]

This is a linear transformation that involves a translation and a scaling. We will need to assume that we can neglect the other  $A_i$  terms with respect to  $A_o$ , and evaluate the effects of this assumption *a posteriori*. In this new space, one can see that  $(y - z) = 0$  and  $(x + t) = 0$ . Therefore, the planes  $(y = z)$  and  $(x = -t)$  have no wind direction modulation. The next step proposed in the transformation is thus a rotation over  $45^\circ$ , and it is expressed as follows:

$$\begin{aligned} X &= \frac{t - x}{\sqrt{2}} = \frac{2\text{COS}(2\phi_2 - 40)}{\sqrt{2}} \\ Y &= \frac{y + z}{\sqrt{2}} = \frac{2\text{COS}(2\phi_2)}{\sqrt{2}} \\ Z &= \frac{t + x}{\sqrt{2}} = 0 \\ T &= \frac{y - z}{\sqrt{2}} = 0 \end{aligned}$$

[Eq:3.5]

In this new space, only X and Y carry information about the wind direction, while Z and T are zero. In the plane of X and Y, the new ‘duplets’ describe what is called a Lissajous curve, which in this case is simply an ellipse inclined 45°, with a ratio R between the lengths of the principle axes. The value of R depends only on the phase difference between the two harmonics and R=2.75 in this case. Therefore, a rotation over 45° and a scaling of the axes by  $\sqrt{R}$  and  $1/\sqrt{R}$  respectively, will transform the curve into a circle. That transformation is expressed for the left swath in [Eq:3.6]

$$\begin{aligned}\eta_1 &= \frac{(X - Y)/\sqrt{2}}{\sqrt{R}} \\ \eta_2 &= \left( (X + Y)/\sqrt{2} \right) \sqrt{R} \\ \eta_3 &= Z/\sqrt{2} \\ \eta_4 &= T/\sqrt{2}\end{aligned}$$

[Eq:3.6]

In order to preserve uniform error characteristics, it is desirable that all the co-ordinates are scaled in a similar way. Therefore, the impact of the difference in scaling by  $\sqrt{R}$  and  $1/\sqrt{R}$  of the first two co-ordinates will have to be studied in the inversion.

The new vector we propose for the inversion is  $\eta=[\eta_1, \eta_2, \eta_3, \eta_4]$ . Figure 3.4(bottom) shows how the model  $\sigma^o$  looks in this transformed space, when not discarding the rest of  $A_i$ . For cross-sections including  $\sigma^o_{2V}$ , the transformed space looks very circular, since we already knew that the  $A_1$  term is negligible with respect to  $A_0$ . When using  $\sigma^o_{2H}$ , we see the impact of  $A_1$  not being so small, by having as a result less circular sections. In any case, we think it is still an improvement over figure 3.4(mid). In Appendix 1 the full measurement space transformation is summarised.

When the inversion is performed in this space, we can assume by good approximation that  $p(\eta_s)$  is constant for varying wind direction. We have now a more optimum space for the inversion. Therefore, we propose a new expression for  $J$  which will maintain the characteristics of the new optimum space in the inversion:

$$J = \sum_{i=1}^N (\eta_{oi} - \eta_{si})^2$$

[Eq:3.7]

It can be seen in figure 3.5(top) that in the sections where the GMF does not fit the data, the transformation is obviously not changing that, since it is purely a linear transformation.

The noise is scaled according to the linear transformation as well and this issue has to be considered carefully. When transforming the measurement space we optimise the inversion by reducing the unwanted non-linearity effects. But in doing so, we are implicitly modifying the noise characteristics to become non-Gaussian. For quasi-linear inversion problems and Gaussian error characteristics, we expect the effect of the

transformation of the noise distribution in the inversion to be of less importance than the geometry of the solution surface (not proven here). However, this assumption for the derivation of  $J$  in the transformed space may be problematic. We think that might be the reason why the results presented in figure 3.2 do not yet look so favourable in the case of NSCAT (not shown here). This question remains open for investigation.

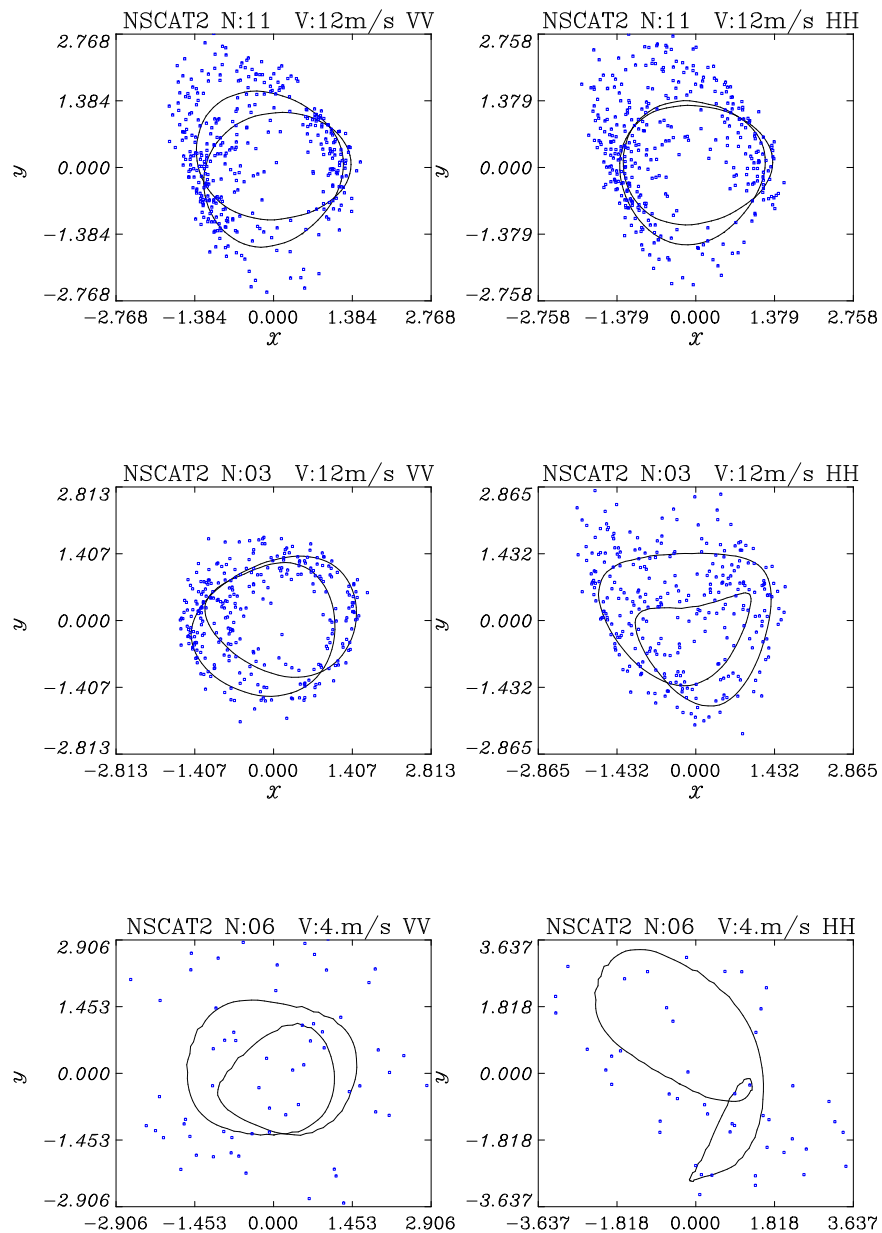


Figure 3.5: Three vertical cross-sections of the NSCAT-2 GMF and NSCAT data transformed measurement space. They correspond to the sections from figure 2.2. The measurements correspond to three days at the beginning of March 97, and they include an incidence angle correction with respect to the average value at that node.



## 4. NSCAT winds Quality Control (QC)

### 4.1. A QC based on the inversion: Justification of the approach

A good assessment of the information content of scatterometer winds is particularly important in order to assimilate them in weather analysis. Lacking other estimation of the quality of scatterometer wind data, the RMS (Root Mean Square) wind vector difference with the model First Guess winds provides a good QC. However, an important requirement for the effective assimilation of data into weather analysis is to have an assessment of their accuracy independent, if possible, from the analysis itself. One possibility to do that in the case of NSCAT winds is to evaluate the wind retrieval performance.

### 4.2. The inversion residual and its normalisation: $R_n$

As introduced in Chapter 3,  $J$  in [Eq:3.1] indicates how well the backscatter measurements used in the retrieval of a particular wind vector fit the GMF, and gives therefore a good indication of the quality (interpretability) of that measurement. The main assumption in the formulation of the problem is related to the GMF, which is empirically determined for fair weather conditions, i.e. average sea state and in the absence of rain. The assumption about the noise of the system through  $SD(\sigma_{si}^o)$  is also very important. The noise is assumed to be Gaussian in  $\sigma^o$  and coming from three different sources: the instrument noise, the measurement collocation error due to the variability of the wind within the WVC, and the uncertainty of the GMF for measurements under the more extreme geophysical conditions. The two former contributions are general and should be taken into account in  $J$ , whereas the more extreme geophysical conditions are specific cases not accounted for in the GMF. Furthermore, the GMF uncertainty is not well known. For that reason, we propose not to include it in the definition of  $J$ . By doing that,  $J$  should spot these cases and we should be able to reject them as bad retrievals.

The best QC indicator would in principle appear to be  $J$  itself. However, figure 4.1 shows that, when using the  $SD(\sigma_{si}^o)$  as specified in the NSCAT product,  $J$  is strongly dependent on wind speed and swath position. Therefore, it cannot be used for quality assessment of NSCAT wind retrievals in their assimilation in weather analysis, since certain wind speeds and swath positions would be penalised systematically. We have normalised  $J$  for any range of wind speed and swath position by its expected value  $J^*$ , which we have formulated as follows:

$$J^*(V, \phi) = \sum_{i=1}^N \left[ \frac{SD^*(\sigma_{si}^o(V, \phi))}{SD(\sigma_{si}^o(V, \phi))} \right]^2$$

$$SD^*(\sigma_{si}^o) = \left\langle \left| \sigma_{oi}^o - \sigma_{si}^o(V, \phi) \right| \right\rangle = \sqrt{SD_{INSTRUMENT}^2(\sigma_{si}^o) + SD_{COLLOCATION}^2(\sigma_{si}^o)}$$

[Eq: 4.1]

where  $SD^*(\sigma_{si}^o)$  represents the expected difference between the observation and the GMF. We have estimated the observation error  $SD^*$  as measurement noise, considering the different contributions as follows.

As instrument noise we have used Cavanié *et al.*, 1997 estimations over arctic sea ice. We have calculated the collocation error using the GMF, after estimating from climate spectrum a wind speed variability within the WVC of 0.5 m/s. The contribution of the GMF uncertainty has not been included in  $SD^*$ , since in case of large GMF error, anomalous geophysical conditions may be present for which the GMF and thus the wind retrieval is invalid. Our purpose is to reject such wind retrievals. Measurements in exceptional geophysical conditions such a confused sea state or rain, are detected by a QC indicator, which we formulate as:

$$R_n = SQRT\left(\frac{J}{J^*}\right)$$

[Eq: 4.2]

Figure 4.1(left) shows how  $J^*$  successfully normalises  $J$  and that  $R_n$  is basically independent of the wind speed and swath position, and therefore a good candidate as a QC indicator for NSCAT winds. At the last reprocessing of the data, JPL modified its measurement noise estimation where the situation improved and  $J$  is now less dependent on wind speed and node (figure 4.1(right)). Also in this case, the normalisation of  $J$  by  $J^*$  is successful. We note that in figure 4.1(left) the NSCAT-1 GMF was used, whereas on the right NSCAT-2 was used.

### 4.3. Correlation between the normalised residual and the departure from ECMWF winds

For every WVC, four wind solutions have been retrieved using NSCAT-2, and their corresponding  $R_n$  values calculated. Because of the symmetry of the problem, in most of the cases we find among them the two main ambiguous solutions with comparable and lowest  $R_n$ . The RMS wind vector departure from the ECMWF wind (ECMWF-RMS) of the 180° wrong main ambiguity is very high and cannot be meaningfully related to the quality of the solution as estimated from the inversion. Therefore, we have carried out our comparison by taking into account only the solutions within 90° of the ECMWF wind vector. About 50% of the solutions are considered through this selection, which confirms our hypothesis that the problem is indeed symmetric. Figure 4.2 shows that ECMWF-RMS and  $R_n$  are fairly well correlated up to  $R_n$  values of 2.5, which supports the use of  $R_n$  as an indicator of the information content of the retrieved solutions. The ‘branches’ at the right side of the plot appear at certain wind directions relative to the satellite track (fig 4.5), and are apparently related to the geometry of the measurement system.

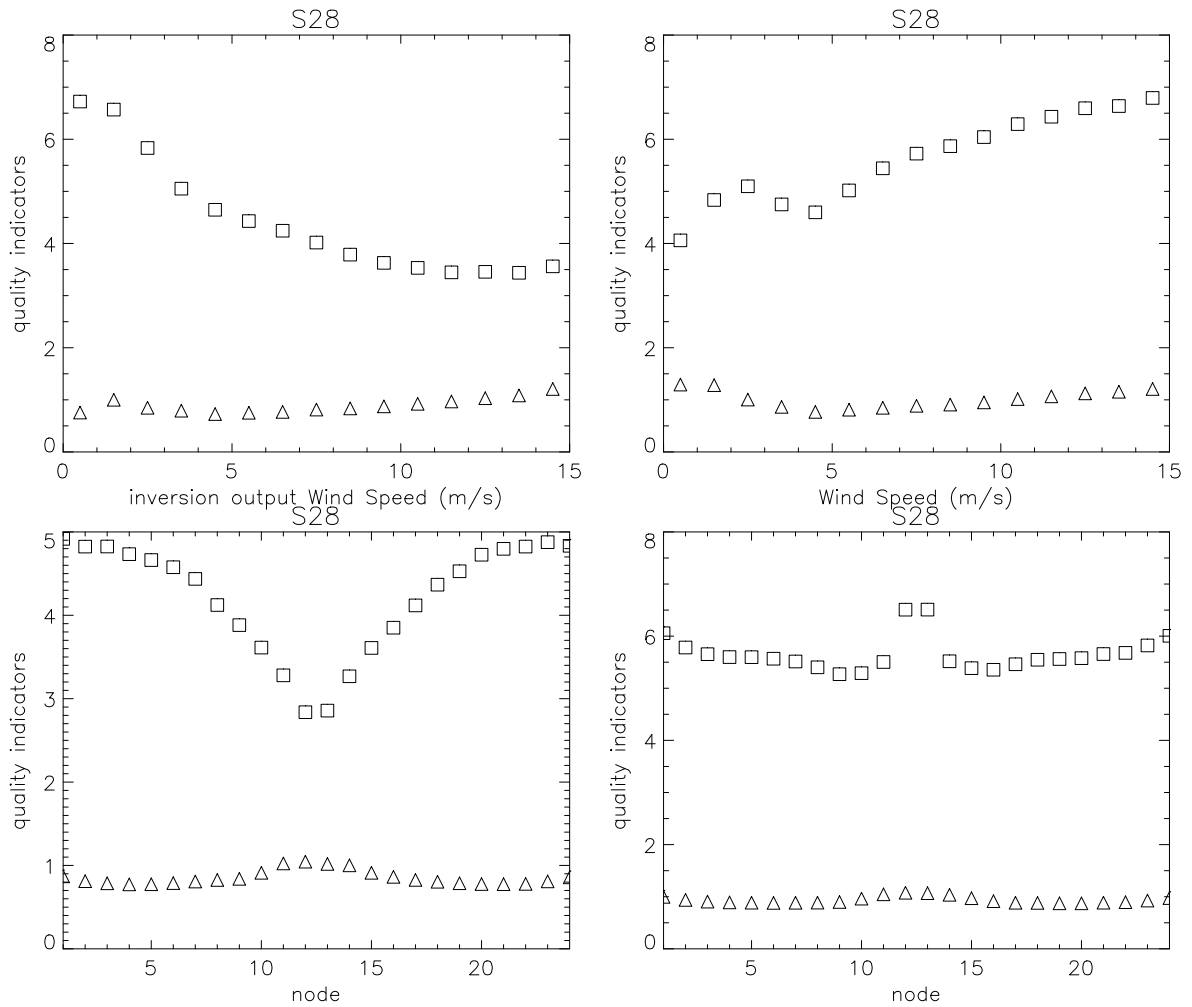


Figure 4.1. (left) Averaged  $\text{SQRT}(J)$  (squares) and  $R_n = \text{SQRT}(J/J^*)$  (triangles) with respect to wind speed (top) and swath position (bottom). The data used correspond to a week of data (batch S28) in March 1997, from the JPL product available in spring 1998 and using NSCAT-1. (right) The same, for latest reprocessed data and the NSCAT-2 GMF, available in September 1997.

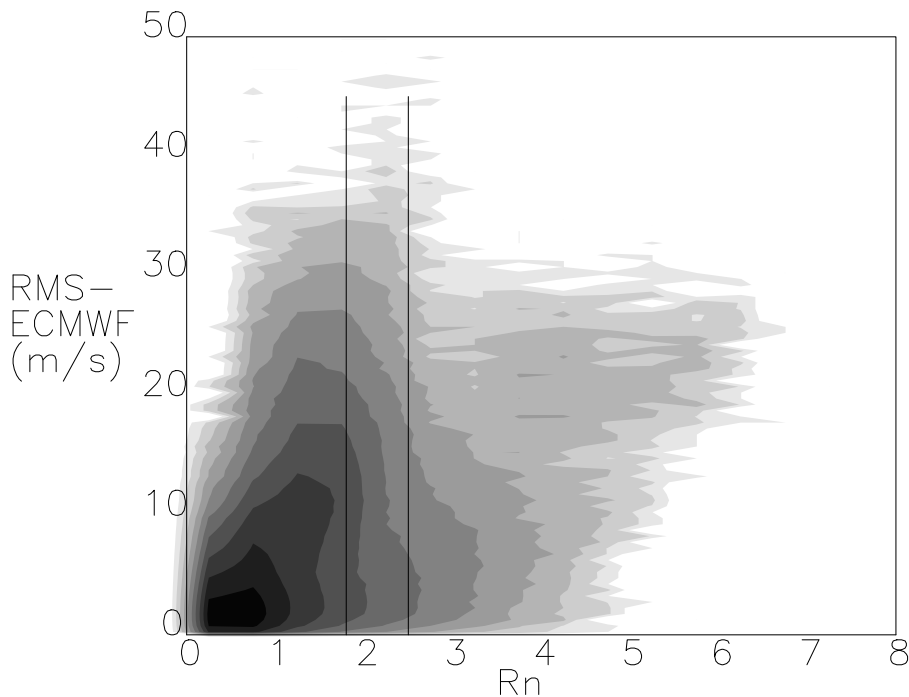


Figure 4.2. Log-histogram of ( $R_n$  vs. ECMWF-RMS) points corresponding to wind solutions retrieved from batch S28. The two vertical lines correspond to  $R_n=1$ . and  $R_n=2.5$ .

$R_n=2.5$  would appear to be the threshold to choose for accepting solutions from the point of view of interpretability. However, when applying that threshold to about 1000000 solutions (one week of data approximately), the average ECMWF-RMS of the accepted solutions is 10 m/s, too high to contribute with meaningful information to the weather analysis. A value of  $R_n=1.8$  accepts solutions with a more reasonable average ECMWF-RMS of 4.5 m/s.

In the case of NSCAT, 95,9% of the solutions are accepted, and 4.1% rejected, the latter with a high average ECMWF-RMS of 10.6 m/s, which again supports the effectiveness of the threshold chosen. The number of nodes with some solution accepted is 98.0%. Some of these have only one solution left or maybe more than one separated less than  $90^\circ$ . These will most likely not be dealt with properly by the ambiguity removal, so we reject them as well (0.6%), losing in total only 2.6% of the nodes. The results are summarized in tables 4.1 and 4.2.

For reference, the operational implementation of roughly the same QC method in the case of ERS-PRESCAT (Stoffelen *et al.*, 1997 (2)), accepts solutions of approximately 3 m/s ECMWF-RMS for  $R_n \approx 3$ . The ERS inversion is less ambiguous and uses a simpler scheme to reduce the number of solutions to two.

WIND SOLUTIONS		avg ECMWF-RMS
accepted	95.92%	4.46 m/s
rejected	4.08%	10.63 m/s

Table 4.1. QC statistics in percentage of solutions and average RMSM-ECMWF, after applying a threshold of  $R_n=1.8$  for rejection to batch S28 data (approximately 1000000 solutions).

WIND NODES		
accepted	98.0%	
rejected	2.0%	
post-rejected	0.6%	2.6% total rejected

Table 4.2. QC statistic in percentage of nodes, after applying a threshold of  $R_n=1.8$  for rejection of solutions to batch S28 data).

#### 4.4. A closer look at the effect of rain

Collocations between the retrieved winds and SSM/I rain data from the NASA Pathfinder data set [Wentz *et al.*, 1996] have been found within 0.25 deg. and 30 minutes. In figure 4.3, it is shown that most of the wind solutions with rain collocations above 12 mm/hr are rejected by  $R_n=1.8$  and correspond to high ECMWF-RMS values (compare with figure 4.2)

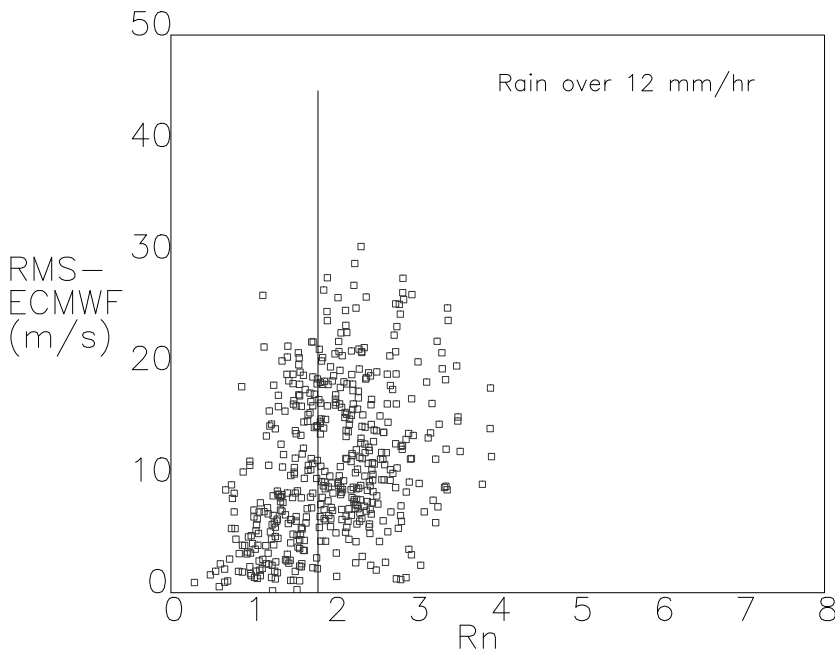


Figure 4.3. ( $R_n$  vs. ECMWF-RMS) points corresponding to wind solutions retrieved from batch S28 where a SSM/I collocation above 12mm/hr has been found. The vertical line corresponds to  $R_n=1.8$ .

#### 4.5. Several cases to illustrate the QC method performance

We have looked at several particular cases to check how the QC performs. Figures 4.4(a) and 4.4(b) show two typical NSCAT passes where the QC has been applied. Erroneous solutions along and across the satellite track appear, but the QC rejects these accepting both main ambiguities. The success of this rejection is better in the mid to inner swath, while in the outer swath all solutions are accepted in most of the cases.

Figure 4.4(c) shows a case of undeveloped sea state in a coastal area, where the wind blows offshore with great force. This is a special sea state that does not correspond to the fair weather conditions for which the GMF has been derived. Many spurious solutions appear in the area, which are rejected by the QC. At a certain distance from the coast, the sea has developed into an equilibrium state with the local surface wind and the rejections disappears. The reason why the rejection occurs so far away from the coast is probably related to the presence of coastal sea ice, since the measurements correspond to high latitudes in winter.

Figure 4.4(d) shows a case of tropical rain, where the GMF sensitivity to wind appears to be anomalous. This figure suggests that the area where the poor solutions appear matches in general the area where rain has been detected by SSM/I. However, the identification of rain-contaminated solutions from SSM/I collocations only, does not seem to correspond always on a node by node basis with the QC, and some nodes are rejected by the QC but do not contain much rain according to the SSM/I product. This points out the difficulty of developing a rain flag based only on rain observations from other sensors.

Figure 4.4(e) shows a case of rain outside the tropics. As expected, low rain rates do not affect the retrieval significantly. In this case the rejected nodes may correspond to the confused sea state associated with the edge of the rain front, where a few poor retrievals are rejected. We have found that rejections appear systematically in this type of situations, as has also been our experience with the ERS scatterometer QC.

In figure 4.4(f) a situation is shown which illustrates the slight increase in the average  $R_n$  value for the inner swath suggested in figure 4.1 (lower panel). In many cases a few spurious solutions appear systematically in the inner nodes. They commonly correspond to high speed winds (above  $15 \text{ ms}^{-1}$ ), as is also suggested by the curve slope towards higher wind speeds in figure 4.1 (upper panel). If we include in figure 4.1 (lower panel) solutions with wind speeds above  $15 \text{ ms}^{-1}$ , the increase of  $R_n$  for the inner nodes is accentuated (plot not shown). We think that this problem has to do with the NSCAT-2 GMF and the formulation of J [Eq:3.1], which might perform less well for the inner nodes at high wind speeds. Fortunately, our QC properly rejects these wrong solutions.

#### 4.6. The wind direction dependency of $R_n$ and ECMWF-RMS

Although  $R_n$  is basically independent of wind speed or swath position, figure 4.5 indicates that the inversion performance is wind direction dependent, as is the ECMWF-RMS. That dependency has a symmetry with respect to the satellite track, and is therefore related to the geometry of the measurement system. As a consequence, the number of solutions depends on the wind direction relative to the satellite track.

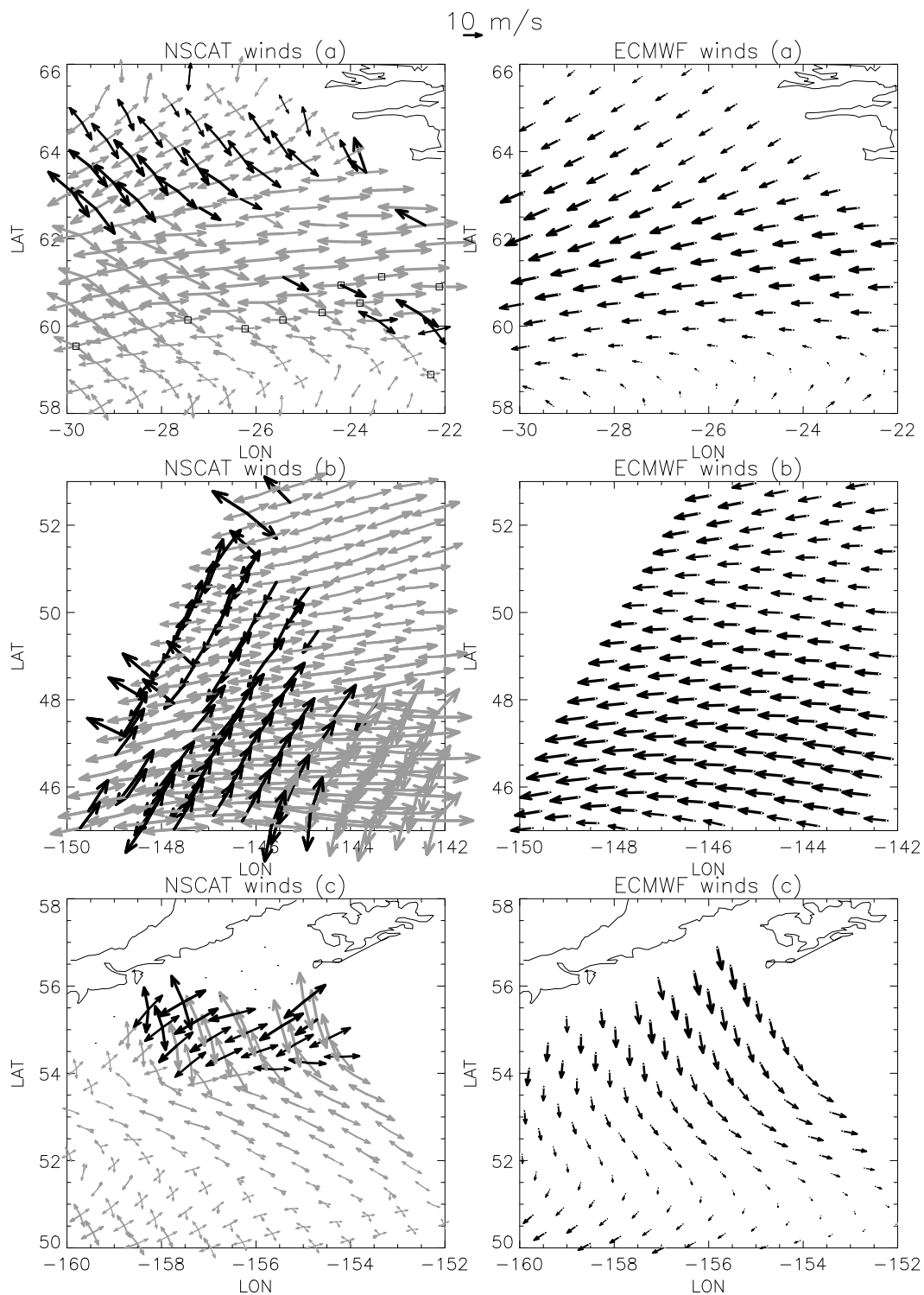


Figure 4.4 (a, b, c). Cases for illustration of how  $R_n$  assesses the information content of individual wind solutions. The left panels show all the solutions retrieved from NSCAT. In grey are the ones accepted by the QC ( $R_n < 1.8$ ) and in black those rejected. The right panels show collocated ECMWF winds for each situation. Collocated SSM/I rain measurements are plotted over as squares, the size of the squares corresponding to the rain intensity. Three sizes are plotted for rain below 3, between 3 and 12 and above 12 mm/hr respectively. The points represent locations for which a SSM/I collocation for NSCAT measurements could not be found.

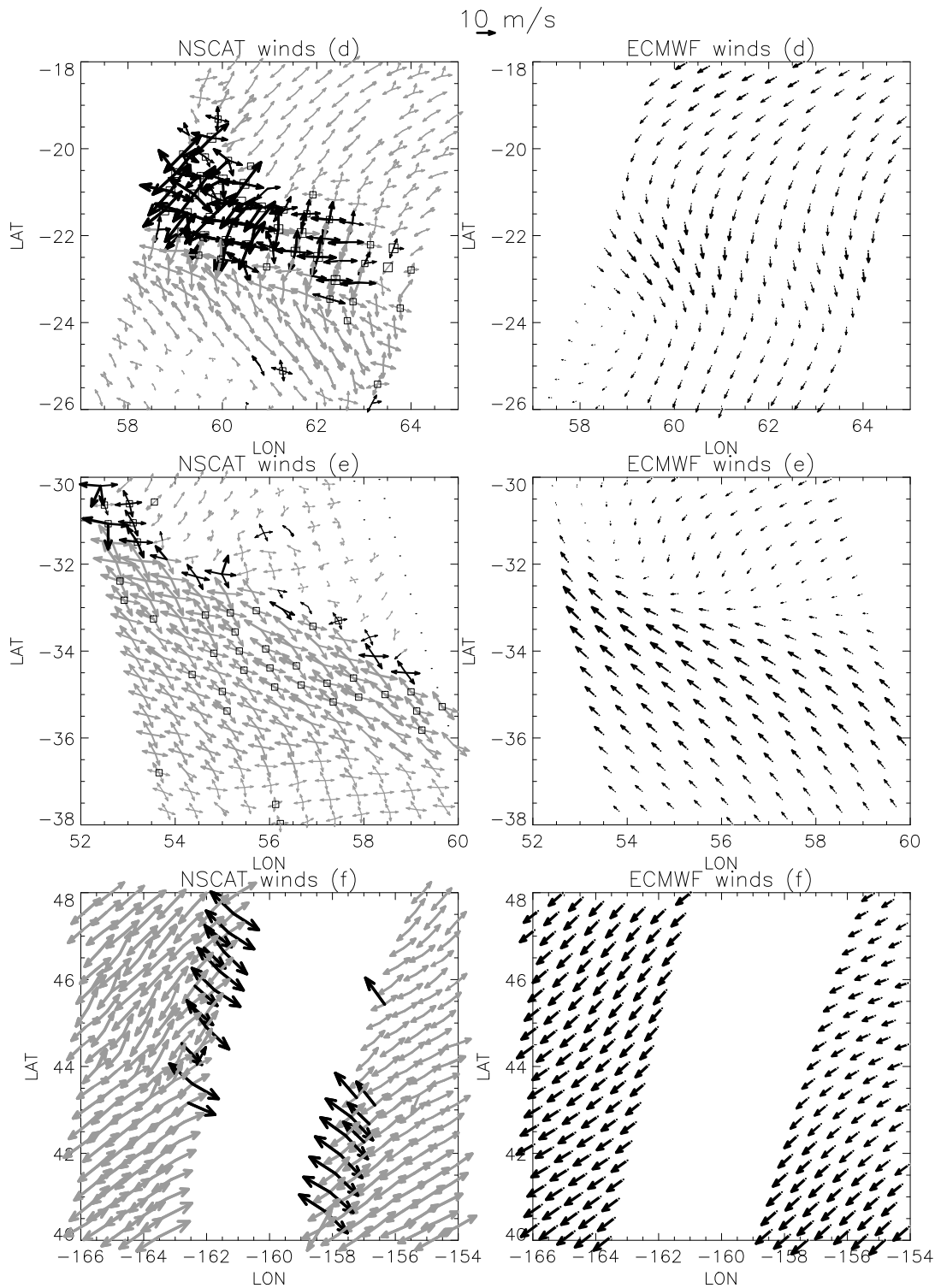


Figure 4.4 (d, e, f). Cases for illustration of how  $R_n$  assesses the information content of individual wind solutions. The left panels show all the solutions retrieved from NSCAT. In grey are the ones accepted by the QC ( $R_n < 1.8$ ) and in black those rejected. The right panels show collocated ECMWF winds for each situation. Collocated SSM/I rain measurements are plotted over as squares, the size of the squares corresponding to the rain intensity. Three sizes are plotted for rain below 3, between 3 and 12 and above 12 mm/hr respectively. The points represent locations for which a SSM/I collocation for NSCAT measurements could not be found.

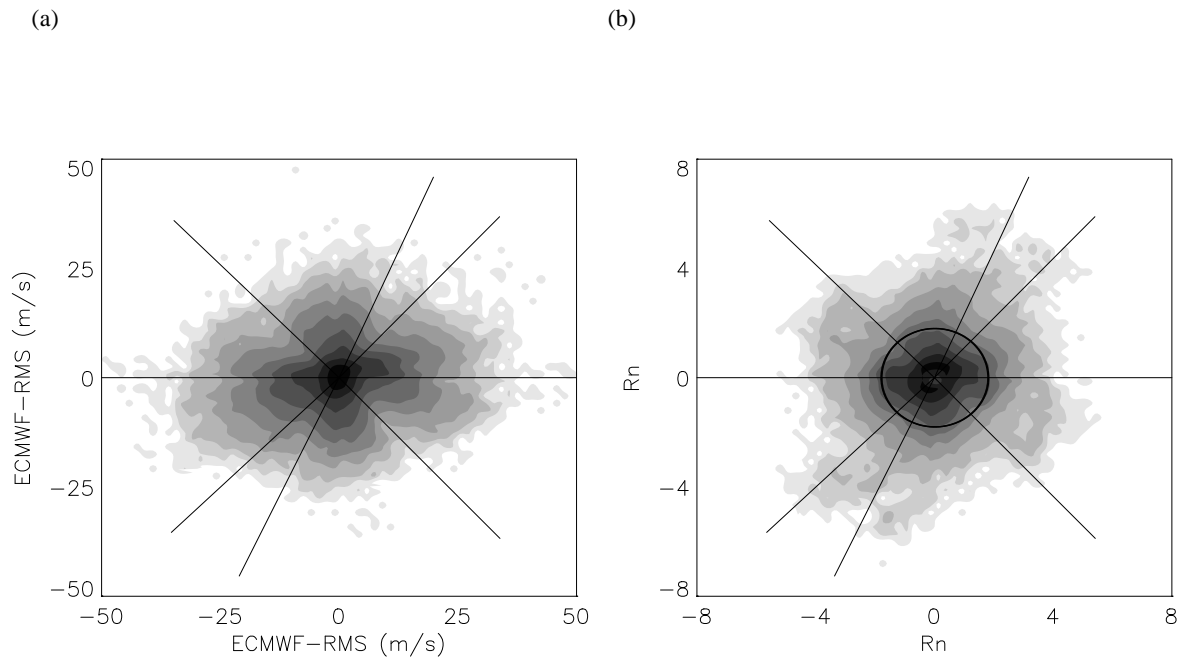


Figure 4.5. Polar plot representing the log-histograms of  $R_n$  and ECMWF-RMS values with respect to retrieved wind direction with respect to the satellite track (black line), for batch S28 of data. The horizontal line represents the satellite direction, and the different antennae azimuths are plotted over. The circle on the right plot corresponds to  $R_n=1.8$ .



## 5. Summary and conclusions

The use of the measurement space is a useful tool to evaluate the  $\sigma^o$  measurements and the GMF. In spite of the noise, the coherence of the measurements around a surface in the 4-D space confirms the assumption that they depend mainly on two geophysical parameters, which are wind speed and direction. That relationship is described through the GMF and conditioned by the geometry of the instrument, i.e. incidence angle and polarisation. This relationship is not perfectly tuned for low incidence angles, where a disagreement between the position of the measurements and the GMF in the 4-D measurement space is found. Elsewhere, the GMF fits the data rather well.

The noise of the measurements at low wind speeds (around 4 m/s) makes it hard to identify whether the measurements lie over the GMF or not. The fact that the geometric centre of the model section matches approximately the geometric centre of the measurements, suggests that the wind speed accuracy of the retrieval will be acceptable. However, the fact that it is not possible to identify where in the GMF section does a noisy measurement lie, indicates that the wind direction retrieval will be very inaccurate for low wind speeds. However, note that wind direction becomes less meaningful at low wind speeds.

Concerning the measurement space transformation, we have proposed a method for NSCAT, which indeed improves the geometric characteristics of the inversion space. However, the wind direction retrieval does not seem to significantly improve in that space. In order to explain why, we are investigating the modifications in the measurement noise characteristics during the transformation process.

We have looked closely at the inversion problem, starting by developing software which successfully simulates the JPL inversion. The main assumptions about the inversion process have been evaluated. One of them is the measurement noise estimation. The fact that, on average, the inversion cost function  $J$  as used with NSCAT-1 by JPL depends on wind speed and node, shows clearly that the  $\sigma^o$  measurement noise model was not realistic. Our noise model, consisting of instrument noise from estimations over sea ice, in addition to  $\sigma^o$  collocation noise within the WVC, is shown to effectively normalise the inversion cost function. Therefore, we think it provides with a more realistic representation of the instrument noise. The new JPL noise model used with NSCAT-2 was empirically tuned and shows an improvement, since  $J$  is less dependent on wind speed and node.

The normalised residual  $R_n$  obtained by using our noise estimation is a quantity and independent of wind speed for the most common range of wind speeds (up to 20 m/s). For higher wind speeds, our noise estimation does not improve the situation with respect to the JPL estimations.  $R_n$  is also independent of node, also for the inner nodes. Therefore, we believe that  $R_n$  represents the quality of the wind retrieval. The good correlation with other quality control indicators, such as the root mean square vector difference with the ECMWF model winds (ECMWF-RMS) confirms that.

Furthermore, the correlation of  $R_n$  with ECMWF-RMS allows us to establish a threshold on  $R_n$  for the rejection of unsuccessful retrievals. By ensuring that the accepted solutions have on average a ECMWF-RMS of about 4.5 m/s, we find a  $R_n$  threshold for rejection of about 1.8. Geophysical effects not modelled by the GMF, such as confused sea state or rain, are in many cases associated with high values of  $R_n$  and can therefore be rejected. This has been verified with collocated SSM/I rain measurements.

The wind direction distribution shows peaks and troughs relative to the satellite orientation. Changes in the inversion space, which provide a more regular solution surface (cone) in the measurement space, seem not to improve the situation noticeably. The wind direction accuracy is still an open issue and more development is needed in order to solve it.

## 6. Ongoing work and plans for QuikSCAT

### 6.1. NSCAT wind direction retrieval

As it has been shown in chapters 3 and 4, there is still work to be done in order to improve the wind direction accuracy of NSCAT winds. In summary, the NSCAT wind direction distribution is aligned with the beam pattern. The normalised residual and the RMS wind vector difference with ECMWF winds are also strongly node dependent.

The probable reason for that is the non-linearity of the inversion problem. The GMF is a non-linear function. The presence of measurement noise in the NSCAT measurement space leads -through a non-linear inversion- to a wind direction distribution, which is not realistic, since it is aligned with the beam pattern. This is, wind direction bias depends on wind direction.

Attempts are being made to find a measurement space transformation where the inversion is less affected by the non-linearity of the problem. In chapter 3, a transformation has been proposed that could suit this requirement. However, if we recall one of the assumptions of the inversion formula, the measurement noise is expected to be Gaussian. It appears that the transformation proposed might be failing that assumption in the new space, because of the way in which the noise is being transformed. We are at present looking into the issue and expect to introduce modifications to the transformations in order to account for this problem.

### 6.2. Impact study of NSCAT winds in weather forecast

In collaboration with ECMWF, a study of the impact of NSCAT winds in weather forecasting and analysis is currently ongoing. The experiment takes place during hurricane Lili, which hit the UK in October '96. The forecast of this and similar extreme weather events is in general not very satisfactory. The lack of data over the ocean, where they develop, is one of the main limitations for the NWP models to give a good prediction of their intensity and position. A spaceborne scatterometer is able to provide accurate winds over the ocean surface and can potentially contribute to improve the situation. Obviously, improvement due to the assimilation of scatterometer data can take place in any weather situation in principle, but it is in an extreme event such as Lili where the impact should be most beneficial, and that is why it has been chosen for this study.

Similar impact studies of the assimilation of ERS winds in NWP [Isaksen *et al.*, 1998] have shown that a positive impact depends very much on the number of times the scatterometer swath hits the developing tropical cyclone and on whether it passes over the centre of the system or outside its limits. The improved time and space coverage of NSCAT with respect to ERS should in principle improve this situation (Stoffelen *et al.*,

1997 (3)). On the other hand, the effect of rain on NSCAT measurements is a concern, since heavy rain episodes are likely to take place within such weather systems.

The NSCAT observation operator fed into NWP consists on up to four ambiguous winds per node and an assessment of the information content of those winds. As shown in chapter 4, the inversion normalised residual  $R_n$  is a good indicator of the quality of each scatterometer wind solution. Additionally, an a-priori estimation of the probability of the wind direction can also be attempted. Without any prior information about the wind direction accuracy of each of the ambiguous solutions, a first estimation of the probability of a certain solution can be related to the angular sector that that particular solution represents, as shown in figure 6.1.

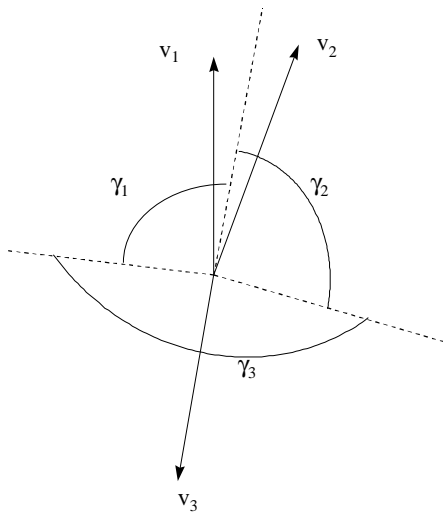


Figure 6.1: Given a number of ambiguous NSCAT solutions, an a-priori estimation of the probability of each of the ambiguous directions  $P(v_i)$  be given as proportional to the angle sector of influence of every direction  $P(v_i) = \gamma_i / 2\pi$

A NSCAT observation operator can be then built up for every node with the winds and their information content and would have a shape similar to figure 6.2.

KNMI provides ECMWF with the information needed to built up the observation operator and ECMWF will perform an impact study in the ECMWF forecast of hurricane Lili.

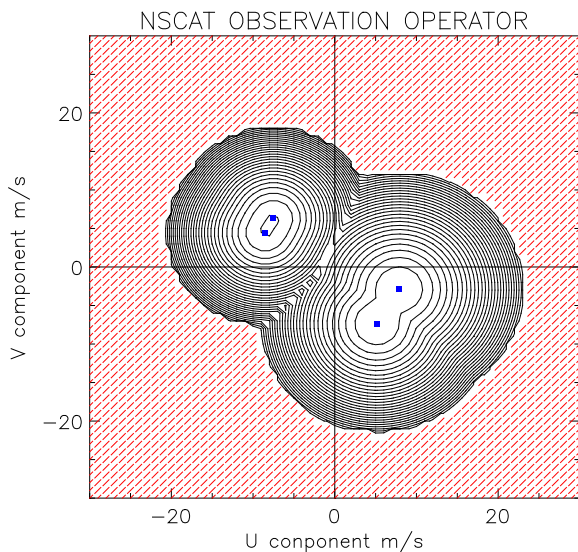


Figure 6.2: Given a number of ambiguous solutions, we propose an observation operator for NSCAT, which accounts for the accuracy of the solution ( $R_n$ ) and the a-priori probability of a particular wind direction ( $P_s$ ). The operator model has been drawn for a typical symmetrical ambiguity, where the  $(v, \phi)$  solutions (in blue) are  $(9.8, 310.0^\circ)$ ,  $(9.6, 207.5^\circ)$ ,  $(9.0, 145.0^\circ)$ ,  $(8.4, 110.0^\circ)$  and their  $R_n$  values 0.27, 0.32, 0.67 and 0.8 respectively. The observation operator gives the probability of a wind vector in the wind components space. It is maximum around the solutions. The area in red corresponds to very small probability. The value of  $R_n$  is used to estimate both the width and the depth of the minima

### 6.3. The new challenges of a scanning scatterometer geometry

SeaWinds on QuikSCAT is the first scatterometer with a rotating pencil beam. Figure 6.3 shows how two beams scan the ocean surface at distances of 700 and 900 km from the satellite nadir point. Their incidence angles are approximately fixed at  $46^\circ$  and  $54^\circ$ . The inner beam provides with a horizontal polarisation measurement and the outer beam with a vertical polarisation one. Each target in areas **I** and **II** over the ocean is viewed twice by each antenna, resulting in four different backscatter measurements [ $\sigma_{HH-FORE}^\circ$ ,  $\sigma_{HH-AFT}^\circ$ ,  $\sigma_{VV-FORE}^\circ$ ,  $\sigma_{HH-AFT}^\circ$ ] per target. The nominal resolution of QuikSCAT is 25x25 km, although it is possible to achieve a higher resolution (6x25 km) by using Doppler shift techniques within the footprint.

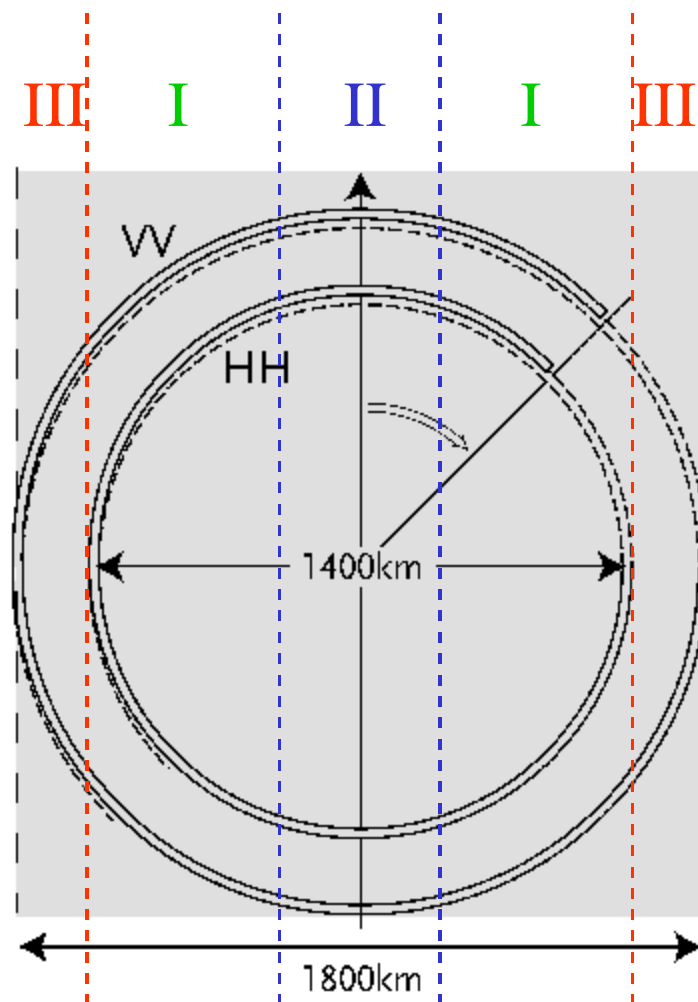


Figure 6.3: SeaWinds viewing geometry. Two scanning rotating antennae with HH and VV polarisation, and  $54^\circ$  and  $46^\circ$  incidence angle respectively. Areas **I**, **II** and **III** represent different parts of the swath where different inversion techniques might have to be applied to retrieve good quality winds.

Following figure 6.3, area *I* are parts of the swath where the same inversion techniques as for NSCAT may be applied successfully, since there are four different backscatter measurements per target. In area *II*, the fore and aft viewing azimuths will be very similar for all four measurements. Therefore, the wind direction retrieval will have poor quality here. In area *III*, two measurements with single polarisation (VV) are available only. We have therefore a situation similar to SeaSAT and resolve the wind direction with much ambiguity. A different inversion technique will have to be developed for the areas *II* and *III*, taking into account the non-linear inversion process.

#### *6.4. Follow-on activities at KNMI*

The results of the work developed through the EUMETSAT NSCAT Fellowship are just the beginning of the KNMI involvement in Ku-band scatterometry. As mentioned, the EUMETSAT QuikSCAT Fellowship starting in February '99 will take the work further into the QuikSCAT new geometry challenge.

On the other hand, the Dutch Remote Sensing Board (BCRS) is investing in a one-year project at KNMI, starting also in February '99, with the objective to investigate an early operational QuikSCAT wind product within the NSCAT-type part of the QuikSCAT swath (figure 6.3)

Finally, the SeaWinds activities within the EUMETSAT NWP-SAF have just started. The objective is to use the available results from the two previous projects to provide the NWP community with a full swath QuikSCAT data assimilation methodology.

## References

**Cavanie A.** Evaluation of Kp on central and lateral antennas of NSCAT over arctic sea ice. Report presented to the 12<sup>th</sup>. ASCAT Science Advisory Group Meeting in Darmstadt, Germany, 16-17 October 1997.

**Isaksen L., Le Meur D., Stoffelen A.** Impact of ERS-Scatterometer wind data on ECMWF's analyses and forecasts of tropical cyclones. Proceedings of the Emerging Scatterometer Applications Workshop in ESTEC, 5-7 October 1998.

**Naderi F.M.** Spaceborne radar measurement of wind velocity over the ocean. An overview of the NSCAT scatterometer system. *Proceedings of the IEEE*. Vol.:79, pp.:850-866, 1991.

**Stoffelen A.** Scatterometry. PhD thesis, Utrecht University, 1998.

**Stoffelen A., Anderson D.** Scatterometer data interpretation: measurement space and inversion. *Journal of Atmospheric and Oceanic Technology*. Vol.:14, pp.:1298-1313., 1997 (1)

**Stoffelen A., Anderson D.** Ambiguity removal and assimilation of scatterometer data. *Q.J.R. Meteorological Soc.*, 123, 491-518, 1997 (3)

**Stoffelen A., Anderson D.** Scatterometer data interpretation: Estimation and validation of the transfer function CMOD4. *Journal of Geophysical Research*, vol102(C3), pp. 5767-5780, 1997 (2)

**Wentz F.J., Peterherych S., Thomas L.A.** A model function for ocean radar cross sections at 14.6 GHz. *Journal of Geophysical Research*. Vol.:89, No.:C3, pp.:3689-3704, 1984.

**Wentz F.J., Smith D.K.** A model function for the ocean normalized cross section at 14 GHz derived from NSCAT observations. Submitted to the *Journal of Geophysical Research*, NSCAT special issue, 1998.

**Wentz F.J., Spencer R.W.** SSM/I rain retrievals within a unified all-weather ocean algorithm. Submitted for *Journal of Atmospheric Sciences*, PIP-2 issue, Feb 1996.



## Acknowledgements

This work has been carried out under the EUMETSAT NSCAT fellowship in the Royal Netherlands Meteorological Institute. I would like to thank Ad Stoffelen for his guidance, ideas and his critical view.

A big part of the software development has been done in the ECMWF computing facilities. Thanks to the user support team for their help. Also thanks to Wim&John in KNMI, this report would not have been printed without their help.

The SSM/I rain data was retrieved from the Remote Sensing Systems web page. The NSCAT data was downloaded from the PODAAC server in JPL.

Thanks to my colleagues in the Satellite Data division for their support, in particular to Paul and Willemien for their reality and unreality checks.



## Acronyms

ASCAT:	Advanced Scatterometer
ECMWF:	European Centre for Medium Range Weather Forecast
ECMWF-RMS:	Root mean square difference with ECMWF wind vectors
ESA:	European Space Agency
EUMETSAT:	European Organisation for Meteorological Satellites
GMF:	Geophysical Model Function
JPL:	Jet Propulsion Laboratory
METOP:	Meteorological Operational Satellite
MLE:	Maximum Likelihood Estimator
NASA:	National Aeronautics and Space Administration
NSCAT:	NASA Scatterometer
NWP:	Numerical Weather Prediction
PODAAC:	Physical Oceanography Distributed Active Archive Center.
PRESCAT:	Pre-processor for Scatterometer data
QC:	Quality Control
RMS:	Root Mean Square
WVC:	Wind Vector Cell



## Annex 1: NSCAT measurement space transformation

The measurement space transformation that we propose in order to improve the wind direction retrieval of NSCAT winds consists of a scaling, a translation and a rotation. It is applied to the measurements vector  $[\sigma_1^o, \sigma_{2V}^o, \sigma_{2H}^o, \sigma_3^o]$  and results in another vector  $[\eta_1, \eta_2, \eta_3, \eta_4]$  in a new space. The new co-ordinates  $\eta_1$  and  $\eta_2$  contain the wind direction modulation. According to the GMF,  $\eta_3$  and  $\eta_4$  are zero. They can therefore be used as a boundary condition that transforms the 4-D problem into a 2-D problem in the  $[\eta_1, \eta_2]$  space.

The transformation can be expressed in a matrix form as follows, where  $A_0, A_2, A_0', A_2', A_0'', A_2''$  are obtained from the GMF according to the geometry of the antenna system.  $R=2.75$  is the axes ratio of a Lissajous ellipse for a phase difference of  $40^\circ$

$$\frac{1}{2} \begin{bmatrix} \frac{-1}{A_2 \sqrt{R}} & \frac{-1}{A_2' \sqrt{R}} & \frac{-1}{A_2'' \sqrt{R}} & \frac{1}{A_2 \sqrt{R}} \\ -\sqrt{R} & \sqrt{R} & \sqrt{R} & \sqrt{R} \\ \frac{1}{A_2} & 0 & 0 & \frac{1}{A_2} \\ 0 & \frac{1}{A_2'} & \frac{-1}{A_2''} & 0 \end{bmatrix} \begin{bmatrix} \sigma_1^o \\ \sigma_{2V}^o \\ \sigma_{2H}^o \\ \sigma_3^o \end{bmatrix} + \frac{1}{2} \begin{bmatrix} \frac{A_0'}{A_2' \sqrt{R}} + \frac{A_0''}{A_2'' \sqrt{R}} \\ \frac{A_0'}{A_2' \sqrt{R}} - \frac{A_0''}{A_2'' \sqrt{R}} \\ -2 \frac{A_0}{A_2} \\ -\frac{A_0'}{A_2'} + \frac{A_0''}{A_2''} \end{bmatrix} = \begin{bmatrix} \eta_1 \\ \eta_2 \\ \eta_3 \\ \eta_4 \end{bmatrix}$$



## Annex 2: NSCAT processing infrastructure developed at KNMI and ECMWF

During the NSCAT EUMETSAT Fellowship work, several processing capabilities have been developed, using both KNMI and ECMWF facilities.

We are able to read the NSCAT JPL-HDF Levels 1.7 and 2.0 products to extract all available information related to 50 km WVC  $\sigma^0$  and winds. The work that is explained in this report has been based in the contents of those products. However, a product based on BUFR format is required for wind assimilation in NWP models. Therefore, encoding and decoding capabilities of NSCAT BUFR format have also been made available.

Although we have access to JPL NSCAT data, we could not gain access to their wind retrieval software. In order to examine the wind retrieval process and establish the QC, we have developed our own inversion software, by adapting ERS-PRESCAT to the NSCAT inversion algorithm. The winds obtained through our software are practically the same as those found in JPL Level 2.0 product, and we are thus satisfied with our simulation of the JPL wind retrieval. Furthermore, in order to study improvements in the wind direction retrieval, the possibility of introducing measurement space transformations is also available in the inversion software.

In order to test the wind retrieval and QC, it is useful to use external information related to the quality of the scatterometer measurements and winds. Collocation files can be built up for that purpose, which include ECMWF First Guess winds and SSM/I rain data. The collocation software is available in the ECMWF server.



## Annex 3: Related presentations and publications

(by Figa J. & Stoffelen A.)

- NSCAT Science Symposium, USA Nov.'97  
Poster: *The retrieval of Quality NSCAT winds*
- EUMETSAT NSCAT Fellowship 1<sup>st</sup>-year presentation, EUMETSAT, Feb '98  
Presentation: *Towards the retrieval of good quality near sea surface winds from NSCAT*
- QuikSCAT GMF committee meeting, USA Mar.'98  
Presentation: *Assessment of the NSCAT-1 Geophysical Model Function and the inversion scheme for NSCAT, by using the 'cone approach'*
- QuikSCAT Pre-launch Workshop, USA Aug.'98  
Presentation and paper in proceedings: *A Quality Control assessment method for NSCAT winds based on the inversion performance*
- Workshop on Scatterometer Applications, ESTEC Oct.'98  
Presentation and paper in proceedings: *Towards an improved Ku-band scatterometer wind product*
- EUMETSAT NSCAT Fellowship Final Presentation, EUMETSAT, Jan '99  
Presentation: *Towards an improved Ku-band scatterometer wind product*
- Paper submitted to the IEEE TGARS Special Issue - Emerging Scatterometer Applications.  
*On the assimilation of Ku-band scatterometer winds for weather analysis and forecasting*
- HIRLAM all Staff Meeting, March 15-17, 1999.  
  
Presentation: *On the assimilation of scatterometer winds for weather analysis and forecasting*



## **Annex 4: Contacts and collaborations with other research groups**

During the development of the fellowship, several contacts and collaboration have taken place between KNMI and other groups involved in scatterometry. The most relevant of them are the following:

- With ECMWF, through the development of an impact study of NSCAT winds in weather forecasting and analysis during hurricane Lili (Oct '97).
- With Atmospheric and Environmental Research Inc. (USA) and NOAA, through the NSCAT and QuikSCAT BUFR format development.
- After several presentations related to our work with NSCAT, KNMI has been invited as a member of the Science Investigators group for NSCAT/QuikSCAT
- In order to trigger the development in GMF-related issues for QuikSCAT, a 'GMF Committee' was set, of which KNMI has taken part.